48th AIAA Aerospace Sciences Meeting
Including the
New Horizons Forum and Aerospace
4 - 7 January 2010, Orlando, Florida

Development of Reduced-Order Models for Feedback Control of Axisymmetric Jets

Aniruddha Sinha*, Andrea Serrani† and Mo Samimy‡
Gas Dynamics and Turbulence Laboratory, The Ohio State University, Columbus, OH, 43235

We present the preliminary steps toward development of reduced-order models for feedback control of a high-speed and high Reynolds number axisymmetric jet. The end goal of the control is two-fold: real-time attenuation of far-field acoustic radiation, *or* enhancement of bulk mixing through increased entrainment of the ambient fluid. The actuation consists of a set of localized arc filament plasma actuators that create controlled perturbations in the initial shear layer of the jet through intense localized Joule heating. The proposed feedback sensing mechanism involves the time-varying pressure information from the irrotational near-field of the jet. We propose to use three-component stereo PIV of several cross-stream slices of the unforced and actuated jets to generate an empirical database of the flow-field. A combination of Proper Orthogonal Decomposition, Stochastic Estimation, and Galerkin Projection is to be used to derive a dynamical model of the jet shear layer from this database. Preparatory to the actual experiments, in this paper we evaluate the proposed modeling strategy using an existing Direct Numerical Simulation database of a similar unforced jet flow.

I. Introduction

Jet noise has been a cause for concern since the commercialization of jet engine technology for civil and military aviation. In recent years, the problem has worsened with increasing number of flights, growth of human settlements around airports, enactment of more stringent regulations, and deployment of significantly noisier high-performance military jets. Although jet noise is a mature research area with a history spanning more than five decades, its practitioners are yet to come to a consensus on the fundamental mechanisms involved.[1] However, a common ground among these divergent viewpoints is the recognition of the importance of the large-scale coherent structures in the jet mixing layer close to the nozzle exit, especially near the end of the potential core.

Moving onto a different application, the hot gases exiting from the jet nozzle undergoes bulk mixing with the ambient fluid, in a process that ultimately leads to dissipation. It is of military interest to enhance this mixing, so that the signature of the jet vanishes quickly. The rate of dissipation is clearly correlated with the dynamics of the large-scale structures in the jet mixing layer.[2]

From the above discussion, one can conclude that the disparate research fields of noise mitigation and bulk mixing enhancement in jets have the large-scale structures as a common denominator. Affecting the turbulence characteristics of flows by manipulating large-scale structures is within the realm of flow control, which is therefore appropriate for both these applications. Flow control itself has amassed a considerable history, which has been the subject of several recent reviews.[3–7]

Localized arc filament plasma actuators (LAFPAs) have been developed and continuously improved for flow control applications at the Gas Dynamics and Turbulence Laboratory at The Ohio State University.[8–11] LAFPAs are capable of generating high-amplitude and high-bandwidth control signals, which are crucial actuator characteristics for controlling high-speed and high Reynolds number flows. LAFPAs provide intense but controlled localized Joule heating to manipulate the large-scale structures in the mixing layer by exciting

*Graduate Student, Dept. of Mechanical Engineering, AIAA Student Member.
†Associate Professor, Dept. of Electrical and Computer Engineering, AIAA Member.
‡The Howard D. Winbigler Professor of Engineering, Dept. of Mechanical Engineering, AIAA Fellow, Corresponding author, samimy.1@osu.edu

the natural instabilities of the jet. Eight of these actuators have been deployed in a uniform azimuthal array at the periphery of the nozzle exit of an axisymmetric Mach 0.9 jet. The effects of various forcing azimuthal modes and frequencies on the response of the mixing layer were investigated in Ref. 11. At particular forcing Strouhal numbers and azimuthal modes of operation, the length of the jet potential core was significantly reduced with an increase in the jet centerline velocity decay rate beyond the end of potential core. The effectiveness of plasma actuation in attenuating far-field noise was explored in Refs. 9 and 12. Noise reduction of 0.5 to over 1.0 dB was observed over a range of forcing Strouhal numbers. Moreover, it was noticed that the higher the forcing azimuthal mode, the higher was the noise attenuation. The above explorations were performed on unheated jets. Significant improvements in effectiveness of the LAFPAs have been observed in heated jets for both mixing enhancement,[13] and noise attenuation.[14] For example, at a temperature ratio of 2.5, an average reduction of about 2 dB was found over a range of downstream and sideline measurement locations. These open-loop forcing results demonstrated that the LAFPAs have significant control authority on high-speed and high Reynolds number jet flows for applications involving both noise attenuation and bulk-mixing enhancement.

The above investigations also showed that the optimal forcing parameters for a certain application may exist in a limited region in parameter-space and that the location of this region may be a function of the operating conditions - e.g. Mach number and temperature ratio. A common technique of rendering a system's performance relatively independent of operating conditions is to incorporate feedback. Closed-loop control of near-wall turbulence for drag-reduction, separation control over high-lift devices, cylinder wake control, cavity tone suppression, etc., in low-speed and low Reynolds number flows have seen intense research activity in recent years. In comparison, the development of feedback control in high-speed and high Reynolds number free shear layers has not received as much attention. This is due to (*a*) the lack of suitable actuators till recently, and (*b*) the increased difficulty in modeling the highly turbulent flows of practical interest. The present work is an attempt to fill this void.

For the current discussion, feedback control may be categorized as model-free or model-based. In *model-free* control, a heuristic is designed based on the known static input-to-output characteristics of the control system.[15–17] Several such controller algorithms have been successfully developed and implemented for the present application.[18] An azimuthal array of eight pressure transducers was placed in the irrotational near-field of the jet to obtain an instantaneous, wavenumber-filtered characterization of the jet mixing layer. The following heuristics, designed based on the known character of the near-field pressure, were found to give good results: (*a*) the optimal forcing frequency for bulk mixing enhancement closely corresponds to the maximum in the RMS of the near-field pressure signal, and (*b*) the optimal forcing frequency for noise attenuation approximately corresponds to the minimum in the RMS of the axisymmetric mode of the near-field pressure signal. After being initialized with sub-optimal forcing parameters, the controllers were able to modify the forcing parameters in real-time to closely reproduce the optimal open-loop behavior with brief transient phases.

In spite of this result, there appears to be considerable room for performance improvement that may be realized with a *model-based* feedback controller, which is the most common paradigm in feedback control. Here, control laws are formulated based on a dynamical model of the relationship between the applied control input and the measured sensor output of the control system. This model typically takes the form of a set of interconnected ordinary differential equations (ODE) describing the time-rate of change of the internal states of the model with the applied control input, along with a static map from the states to the sensor measurements. The motivation for moving to a *model-based* approach is three-fold: (*a*) to gain a deeper understanding of the physics involved[5] in the unforced jet, the forced jet, and the plasma actuation itself, (*b*) to attain faster convergence to the optimal parameter regime than the case of model-free control,[19] by incorporating a knowledge of the dynamics of the jet mixing layer in the model, and (*c*) to achieve improvements in power consumption.[20]

From the point of view of practical implementation, as well as the feasibility of actual design of the control law, it is essential that a small set of ODEs be able to approximately describe the dynamical behavior of the control system. However, the 'exact' dynamics of flows are governed by the infinite-dimensional Navier-Stokes equation. Hence, any model-based flow control strategy must necessarily involve the development of a reduced order model (henceforth ROM) of the flow. A number of methods have been employed to develop ROMs of flows of practical interest - they lend themselves to the following broad categorization.

1. Phenomenological models of flows are obtained by invoking intuitive arguments about the essential physics of the flow. Recent examples include the models of flows dominated by oscillations.[19, 21–23]

Unfortunately, the unforced high Reynolds number jet mixing layer is relatively disorganized and this makes the task of phenomenological modeling quite difficult. On the other hand, the coherent structures in the mixing layer have been found to become quite well-organized by forcing near the optimal frequency for bulk mixing enhancement.[8,11] This holds out the hope for phenomenological modeling in the present application.

2. Black-box modeling involves starting with an assumed structure of the ROM (number of dynamic states, degree of nonlinearity, form of the forcing term, etc) before performing well-designed experiments or simulations to identify the dynamical relation between the system input and output.[24] Several implementations have been reported in the recent flow control literature.[25–28] This modeling approach does not incorporate much physical information about the flow, but may be the most viable option in particularly complicated applications.

3. The Galerkin procedure involves two steps to arrive at the ROM.[29] In the first step, the kinematics of the flow are assumed to reside on a low-dimensional manifold, so that the infinite dimensional flow variables are represented by an expansion on a finite number of modes. This expansion is usually linear, but nonlinear expansions have been found to yield greater accuracy for certain flows in bounded domains.[30,31] In the next step, the dynamics of these modes are also assumed to reside on the same low-dimensional manifold, and this is enforced by the Galerkin projection (GP) of the Navier-Stokes equations onto this manifold. Depending on the origin of the expansion modes, Galerkin models have been categorized as mathematical, physical, or empirical.[22] Empirical Galerkin models, as the name suggests, derive their modes from experimental data or numerical simulations. They have been generally found to be the most accurate while employing the least number of modes.[22]

The most common technique of deriving modes from empirical data is the Proper Orthogonal Decomposition (POD).[29,32] Its popularity stems from the fact that it is a linear procedure, and it objectively educes an orthogonal set of basis functions that optimally converges in the sense of a suitably-defined $\mathcal{L}_2$ norm of the projection error. The eduction of POD bases for axisymmetric jets was pioneered in Ref. 33 with several important contributions in recent years.[34–37]

Based on the above discussion of the available options for deriving ROMs, we decided to use POD and empirical GP for our feedback control application. POD-GP has been used for studying the dynamics of flows over the past 20 years; among them we make reference to several pertinent studies.[38–43] In particular, in our lab, we have already implemented a model-based feedback controller for reducing cavity tones using this modeling strategy.[20,44,45]

There are three recent works on the development of numerical simulations of the actuated jet.[46–48] The extremely short time-scale and high energy-density involved in the plasma actuation along with the high-speed and high Reynolds number of the jet make it a difficult problem to simulate. While simulations have been successful in reproducing some aspects of the experiments, none of the above efforts have demonstrated sufficient fidelity. Thus the empirical database has to be obtained from experiments. Present experimental techniques can capture snapshots of the three-components of the velocity field on planar slices of the flow using stereo-PIV. However, it is quite infeasible to obtain simultaneous snapshots of the density and/or pressure field in the same domain. This implies that one is forced to make an *incompressibility* assumption in approximating the Navier-Stokes equations for this flow. A control-oriented model only needs to be *good enough* for representing the short-time-horizon dynamical relation between control inputs and sensor outputs; it need not be accurate enough for long-time-horizon numerical simulation of the flow.[7] Therefore, assumptions like the one above may be justified in the present modeling effort.

Even after one has decided upon using the POD to educe a low-dimensional basis of the flow, a large number of options are open depending on the simplifying assumptions that are made. A very useful (and, in fact, indispensable) tool for evaluating the various strategies is a time- and spatially-resolved 3D volumetric database of the axisymmetric jet. Freund[49] has performed a direct numerical simulation (DNS) of an unforced Mach 0.9 axisymmetric jet with Reynolds number based on jet diameter (Re) of 3600. In spite of its low Reynolds number, most of its general characteristics were found to be similar to those of a jet with a much higher Re.[50] Our experimental jet also operates at Mach 0.9 although its $Re \approx 640,000$. Thus, in this paper, we employed this DNS database to assess various strategies for developing an ROM of the unforced axisymmetric jet.

There are two major stages in the proposed feedback control strategy that should be discussed at this point. The first stage is the development of the model of the flow. This is necessarily a one-time off-line

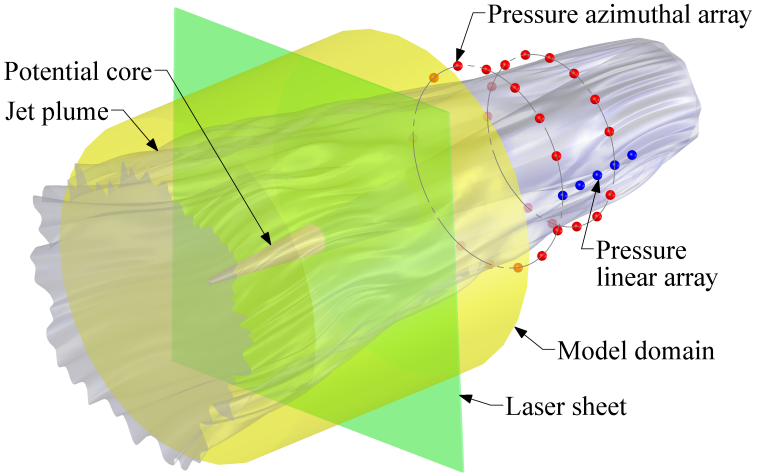

Figure 1. Schematic of axisymmetric jet.

procedure, and these factors afford some freedom in the realm of possible experimental methods. However, the ROM must ultimately be derived from experiments, and so this must always be kept in mind even though we focus on the DNS database in the present paper. The other stage of feedback control is the real-time online operation of the controller. This places considerable constraints on the available options for practical implementation. The current work is quite preliminary, and it does not address this second stage at all. An experimental setup that was found to be suitable for the *model-free* feedback control approach has been described before,[18] and this might serve as a guide in the current endeavor.

In Sec. II, we provide a detailed discussion of the proposed strategy for building the ROM, while leaving various options open for later assessment. In Sec. III, these strategies are applied to the DNS database, and the results of simulation of the various ROMs are employed to determine the most suitable modeling strategy. The paper is concluded with Sec. IV.

II. Steps in Control-Oriented Model Development

A common theme in the application of POD-GP to 3D flows has been the assumption that two of the directions are homogenous, and only one direction is inhomogeneous;[38,39,41] a notable exception is the fully inhomogeneous 3D-POD applied to a numerical database of the cylinder wake.[51] For the axisymmetric jet, the azimuthal and streamwise directions were assumed to be homogenous, with the radial direction being inhomogeneous[39] . Whereas the homogeneity of the azimuthal direction is obvious, our preliminary experience with the DNS database indicated that the streamwise homogeneity assumption is not appropriate for the current modeling purpose. In such a situation, there are two options available. In the original direct implementation of POD,[32] two-point cross-correlations are required for all velocity components for all possible point-pairs over the 3D region of the mixing layer. This poses significant challenges due to the sheer amount of effort that would be involved. In the alternative snapshot formulation,[52] *simultaneous* 3-component flow information is required over the 3D region at different time instants.

The latter option might seem a more difficult proposition, but Refs. 37 and 53 presented an approximation to such 3D snapshots using the technique of spectral linear stochastic estimation (SLSE), and we would adopt this in our work. Briefly, the dynamic pressure was recorded in a time-resolved manner on an azimuthal ring array in the irrotational near-field of the jet (see Fig. 1). Also, at known time instants of the pressure record, the 3-component velocity field was captured on a cross-stream slice using stereo-PIV. Enough of these snapshots were taken for statistical convergence of the two-point second-order statistics. This exercise was repeated for several different cross-stream slices, always measuring the pressure at the same location. Subsequently, SLSE was used to reconstruct the required velocity field using the pressure as the unconditional variable.

In the following sub-sections, we propose a procedure to obtain an ROM for the ultimate purpose of feedback control of an axisymmetric jet. The present paper deals with the unforced flow, without introducing the effects of an actuator. One of our contributions is to rigorously prove and enforce the symmetries of the

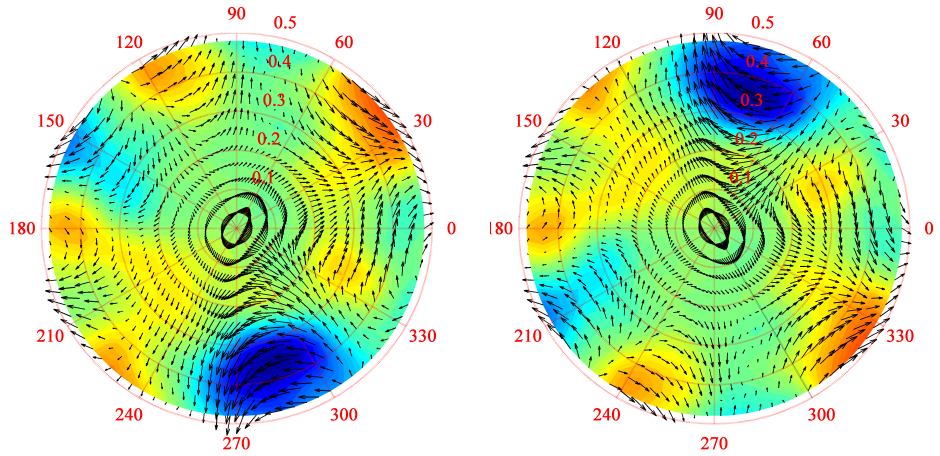

Figure 2. Enforcing axisymmetry. (a) Actual velocity field realization. (b) Corresponding *co-velocity* field.

kinematics of the axisymmetric jet mixing layer. These symmetries (*a*) augment the database collected from experiments, (*b*) make computations easier, and (*c*) model the flow more accurately.[52]

II.A. Normalizations

Let the jet exit velocity and nozzle exit diameter be U_{jet} and D, respectively. Henceforth, all velocities and linear coordinates will be implicitly normalized by these respective quantities. Similarly, time will be normalized by the flow time scale $t^+ := D/U_{jet}$. Pressure is normalized by $\rho_\infty U_{jet}^2$, where ρ_∞ is the ambient fluid density. With the kinematic viscosity of the ambient fluid denoted as ν_∞, the pertinent Reynolds number is defined as $Re := U_{jet}D/\nu_\infty$.

II.B. 1D Proper Orthogonal Decomposition on Cross-Stream Slices

II.B.1. The Setup

The first step is the eduction of a low-dimensional basis for the velocity field at a given cross-stream slice of the axisymmetric jet mixing layer. Ref. 37 is followed closely, with some additional investigation of the symmetries of the problem.

Suppose that the three components of velocity are known on a cross-stream slice of the axisymmetric jet at several time instants, as shown in Fig. 1. The velocity vector is presented in cylindrical coordinates (x, r, θ), with the axial coordinate serving to parameterize the cross-stream slice location. Then the streamwise velocity component is denoted as $V_x : [0, R] \times \mathbb{T} \times \mathbb{R} \times \mathcal{X}_v \to \mathbb{R}$, $V_x : (r, \theta, t; x) \mapsto \mathbb{R}$. Here, R is the radial extent of the measurement domain, $\mathbb{T}$ is the circle group, and $\mathcal{X}_v$ is the set of axial locations of the cross-stream slices. The radial (V_r) and azimuthal (V_θ) components are defined similarly, so that the flow velocity vector is $\mathbf{V} := (V_x, V_r, V_\theta)^T \in \mathbb{R}^3$. The time-stationarity and axisymmetry of the jet are used to define the mean velocity field as $\overline{\mathbf{V}}(r; x) := E\left\{(1/2\pi)\int_{-\pi}^{\pi} \mathbf{V}(r, \theta, t; x)\mathrm{d}\theta\right\}$. Henceforth, unless otherwise mentioned, the expectation operator $E(\cdot)$ will signify the ensemble-average over all realizations indexed by t. Intuitively, $\overline{V}_\theta \approx 0$, and this is enforced explicitly in the implementation. The fluctuating velocity vector is defined as $\mathbf{v}(r, \theta, t; x) := \mathbf{V}(r, \theta, t; x) - \overline{\mathbf{V}}(r; x)$, with the three components being v_x, v_r, and v_θ, respectively.

The axisymmetry of the jet can be used to infer a symmetry condition. Consider an actual realization of the fluctuating vector field $\mathbf{v}$ shown in Fig. 2(a). The contour-map indicates the streamwise component, whereas the vector field is in the cross-stream plane. In a perfectly axisymmetric jet, if one has collected enough realizations, one should also expect to capture the simulated *co-velocity* field $\underline{\mathbf{v}}$ shown in Fig. 2(b), obtained by reversing the measurement convention of the azimuthal coordinate, and inverting the sign of the azimuthal component. Basically, this is another way of saying that the jet does not have a preferred azimuthal direction.[36] Of course, in an actual experiment, one cannot expect to collect both realizations. However, the collected database of realizations can be extended by appending the counterpart of each physical realization

after applying the above transformations. This concept is made precise in the following relations

$$\underline{v}_x(r,\theta,t;x) := v_x(r,-\theta,t;x), \quad \underline{v}_r(r,\theta,t;x) := v_r(r,-\theta,t;x), \quad \underline{v}_\theta(r,\theta,t;x) := -v_\theta(r,-\theta,t;x). \tag{1}$$

It is well-established[32,54] that in the presence of a homogeneous and/or periodic direction in a flow, its POD devolves into the Fourier decomposition along that direction. The azimuthal Fourier transform of a function $f(\theta)$ will be denoted by $f(\theta) \xrightarrow{\mathcal{F}_m} \hat{f}(m)$; $\hat{f}(m) := (1/2\pi)\int_{-\pi}^{\pi} f(\theta)\mathrm{e}^{-\mathrm{i}m\theta}\mathrm{d}\theta$. Here m is the azimuthal mode. The inverse Fourier transform will be denoted by $\hat{f}(m) \xrightarrow{\mathcal{F}_\theta} f(\theta)$; $f(\theta) = \sum_{m=-\infty}^{\infty} \hat{f}(m)\mathrm{e}^{\mathrm{i}m\theta}$. Using this, we define the azimuthal Fourier transform of the fluctuating velocity field as $\mathbf{v}(r,\theta,t;x) \xrightarrow{\mathcal{F}_m} \hat{\mathbf{v}}(r,t;x,m)$. Since $\mathbf{v}$ is real, $\hat{\mathbf{v}}$ is Hermitian in m.

II.B.2. Symmetries of the Cross-Correlation Tensor

The two-point cross-correlation tensor appears as the kernel of the POD problem; it is defined as

$$\Pi_{ij}(r,r',\vartheta;x) := E\left\{\frac{1}{2\pi}\int_{-\pi}^{\pi} v_i(r,\theta,t;x)v_j(r',\theta+\vartheta,t;x)\mathrm{d}\theta\right\}, \quad \forall i,j \in \{x,r,\theta\}. \tag{2}$$

Here we have used the homogeneity assumption to average over the azimuthal domain and to indicate the functional dependence of the correlation tensor on the azimuthal separation (ϑ) alone. The axisymmetry condition of the jet established in (1) can be used to show that the azimuthal shear stresses are odd functions of ϑ, whereas all other correlation coefficients are even functions of ϑ; that is,

$$\Pi_{ij}(r,r',\vartheta;x) = \Pi_{ij}(r,r',-\vartheta;x), \qquad \forall\ (i,j) \in \{(x,x),(r,r),(\theta,\theta),(x,r),(r,x)\}, \tag{3a}$$
$$\Pi_{ij}(r,r',\vartheta;x) = -\Pi_{ij}(r,r',-\vartheta;x), \qquad \forall\ (i,j) \in \{(x,\theta),(r,\theta),(\theta,x),(\theta,r)\}. \tag{3b}$$

Such symmetries have indeed been verified in experiments.[35–37]

The Fourier transform of Π_{ij} is defined in the usual manner $\Pi_{ij}(r,r',\vartheta;x) \xrightarrow{\mathcal{F}_m} \mathcal{B}_{ij}(r,r';x,m)$. The properties of Π_{ij} established in (3b) bestow the following symmetries upon $\mathcal{B}_{ij}$:

$$\mathcal{B}_{ij}(r,r';x,m) = \mathcal{B}^*_{ij}(r,r';x,-m), \quad \forall i,j \in \{x,r,\theta\}, \tag{4a}$$
$$\mathcal{B}_{ij}(r,r';x,m) = \mathfrak{R}\left\{\mathcal{B}_{ij}(r,r';x,m)\right\}, \quad \forall\ (i,j) \in \{(x,x),(r,r),(\theta,\theta),(x,r),(r,x)\}, \tag{4b}$$
$$\mathcal{B}_{ij}(r,r';x,m) = \mathrm{i}\,\mathfrak{I}\left\{\mathcal{B}_{ij}(r,r';x,m)\right\}, \quad \forall\ (i,j) \in \{(x,\theta),(r,\theta),(\theta,x),(\theta,r)\}. \tag{4c}$$

Here $\mathfrak{R}(\cdot)$ and $\mathfrak{I}(\cdot)$ respectively denote the real and imaginary parts of a complex quantity, and $\mathrm{i} = \sqrt{-1}$. The asterisk denotes a complex-conjugate transpose.

In practice, we used the following relation to compute $\mathcal{B}_{ij}$[55]

$$\mathcal{B}_{ij}(r,r';x,m) = E\left\{\hat{v}_i^*(r,t;x,m)\hat{v}_j(r',t;x,m)\right\}, \quad \forall i,j \in \{x,r,\theta\}. \tag{5}$$

Subsequently, we ignored the real parts of the azimuthal shear stresses and the imaginary parts of the remaining correlation coefficients after verifying that they are indeed negligible; the latter has been validated by previous researchers.[37] In the past, analogous symmetries have been enforced on the kernel of a POD performed on a fully-developed channel flow.[56]

II.B.3. The POD Problem and its Symmetries

One defines the *vector* inner-product as[34–37]

$$\left\langle \hat{\mathbf{v}}^{(1)}\ ,\ \hat{\mathbf{v}}^{(2)} \right\rangle := \int_0^R \hat{\mathbf{v}}^{(2)*}\hat{\mathbf{v}}^{(1)} r\mathrm{d}r, \tag{6}$$

where $\hat{\mathbf{v}}^{(1)}$ and $\hat{\mathbf{v}}^{(2)}$ denote two arbitrary fields. Then the *vector* slice-POD can be shown to be the following integral eigenvalue problem

$$\int_0^R \mathcal{B}^*_{ij}(r,r';x,m)\hat{\phi}^{(n)}_j(r';x,m)r'\mathrm{d}r' = \Xi^{(n)}(x,m)\hat{\phi}^{(n)}_i(r;x,m), \quad \forall i \in \{x,r,\theta\}. \tag{7}$$

The quantities $\Xi^{(n)}(x,m)$ and $\hat{\phi}_i^{(n)}(r;x,m)$ are respectively the eigenvalues and the ith component of the eigenfunctions for each POD mode n, parameterized by the streamwise location x and azimuthal mode m; the latter are also functions of the radial coordinate r.

The *scalar* inner product is defined likewise for the ith components of the velocity field:

$$\left\langle \hat{v}_i^{(1)} \ , \ \hat{v}_i^{(2)} \right\rangle := \int_0^R \hat{v}_i^{(2)*} \hat{v}_i^{(1)} r \mathrm{d}r, \quad \forall i \in \{x, r, \theta\}. \tag{8}$$

Then, the *scalar* slice-POD problem is

$$\int_0^R \mathcal{B}_{ii}^*(r,r';x,m) \hat{\varphi}_i^{(n)}(r';x,m) r' \mathrm{d}r' = \xi_i^{(n)}(x,m) \hat{\varphi}_i^{(n)}(r;x,m), \quad \forall i \in \{x, r, \theta\}. \tag{9}$$

Here the eigenfunctions $\hat{\varphi}$ are akin to those for the vector POD, but one obtains individual eigenvalues ξ for the different components of velocity. We will compare the results from the vector and scalar POD later; the reader is referred to other works that provide a more general discussion.[37,43]

The solutions of the POD problem have many salient properties that have been discussed in depth elsewhere;[29,43] here we will only note some of the additional properties that result from the axisymmetry of the flow. In (4a), it has been established that the kernel of the vector POD problem is a Hermitian function of m. Then it readily follows that the eigensolutions themselves are also Hermitian functions of m. Moreover, the properties of the kernel described in (4b) and (4c) can be used to show that the eigenfunctions can always be normalized such that their axial and radial components are real and the azimuthal component is purely imaginary. That is,

$$\Xi^{(n)}(x,m) = \Xi^{(n)}(x,-m) \tag{10a}$$

$$\hat{\phi}_i^{(n)}(r;x,m) = \hat{\phi}_i^{(n)*}(r;x,-m), \quad \forall i \in \{x, r, \theta\} \tag{10b}$$

$$\hat{\phi}_i^{(n)}(r;x,m) = \mathfrak{R}\left\{\hat{\phi}_i^{(n)}(r;x,m)\right\}, \quad \forall i \in \{x, r\} \tag{10c}$$

$$\hat{\phi}_\theta^{(n)}(r;x,m) = \mathrm{i}\ \mathfrak{I}\left\{\hat{\phi}_\theta^{(n)}(r;x,m)\right\}. \tag{10d}$$

One can solve the eigenvalue problem for $m \geq 0$ only; the results for $m < 0$ can be recovered using the above symmetries. The solutions for the scalar POD problem satisfy identical relations; hence they are not repeated.

The 1D POD problem is solved in the discrete radial domain; typically, the number of radial grid points are far fewer than the number of snapshots so that the original (or direct) POD method is employed.[57] The special symmetries of the kernel established above actually allow an equivalent POD problem to be solved entirely in the real number domain, thereby avoiding the computational overhead involved in the use of complex numbers.

II.B.4. POD Modal Coefficients and their Symmetries

The eigenfunctions recovered from the POD can be used to reconstruct the velocity field in the azimuthal Fourier transform domain. The properties of the POD allow us to completely recover any of the velocity field realizations that formed the original database using a linear combination of all the eigenfunctions. We now assume that *any* velocity field $\hat{\mathbf{v}}(r,t;x,m)$ can be approximately reconstructed using the first $N_{n,1}$ eigenfunctions only. For the vector POD, we can write[29,32]

$$\hat{\mathbf{v}}(r,t;x,m) \approx \sum_{n=1}^{N_{n,1}} \hat{\beta}^{(n)}(t;x,m) \hat{\boldsymbol{\phi}}^{(n)}(r;x,m). \tag{11}$$

where, the vector POD modal coefficients are defined as

$$\hat{\beta}^{(n)}(t;x,m) := \left\langle \hat{\mathbf{v}}(r,t;x,m) \ , \ \hat{\boldsymbol{\phi}}^{(n)}(r;x,m) \right\rangle. \tag{12}$$

Analogous relations for the scalar POD are

$$\hat{v}_i(r,t;x,m) \approx \sum_{n=1}^{N_{n,1}} \hat{\gamma}_i^{(n)}(t;x,m) \hat{\varphi}_i^{(n)}(r;x,m), \quad \forall i \in \{x, r, \theta\}, \tag{13}$$

with the scalar POD modal coefficients defined as

$$\hat{\gamma}_i^{(n)}(t;x,m) := \left\langle \hat{v}_i(r,t;x,m)\ ,\ \hat{\varphi}_i^{(n)}(r;x,m) \right\rangle, \quad \forall i \in \{x,r,\theta\}. \tag{14}$$

We have previously established that the velocities as well as the POD eigenfunctions in the Fourier azimuthal domain are Hermitian functions of m; this makes all the modal coefficients similarly Hermitian.

II.C. 3D Velocity Field Reconstruction using Spectral Linear Stochastic Estimation

Stochastic Estimation was originally introduced to educe coherent structures in turbulent flows.[58] Since then, it has also been employed for estimating velocity fields using minimal measurements and a knowledge of the spatial correlations in the flow.[59] The original technique estimated the velocity directly.[60] In the *complementary* technique, the POD modal coefficients of the velocity field were estimated instead.[61] The *modified* complementary technique was introduced for flows having a homogenous direction; it performed the correlation between the unconditional and conditional flow variables in the Fourier transform domain of the homogenous direction.[62] The successive modifications were implemented to take advantage of the increased correlations between the low-dimensional quantities, thereby reducing computations without sacrificing (or, in some cases, actually improving) the accuracy of reconstruction. The spectral variant, SLSE, was implemented for time-stationary flows, where the correlation was computed in the temporal Fourier domain.[53,60,63] This was shown to be especially useful whenever (*a*) the spectral features of the conditional and unconditional variables were disparate, and (*b*) significant time delays existed between the them.[63] Both these effects are manifest in the present application.

As mentioned previously, we adopted the SLSE technique described in Ref. 53. The original work relied on a single azimuthal array of pressure sensors, but we found that the reconstruction can be made more accurate by adding a streamwise linear array of pressure sensors, at little extra cost. Fig. 1 shows an even more general arrangement of pressure sensors that is used to formulate the problem. Consider several azimuthal arrays of pressure transducers arranged at different axial locations $x \in \mathcal{X}_p^a$. In addition, suppose that there are individual pressure sensors at some axial locations $x \in \mathcal{X}_p^l$ that do not belong to any azimuthal array. Although the development does not need the individual sensors to form a linear array; they would be assumed to be in a straight line at $\theta = 0$ for notational convenience. Without loss of generality, it is also assumed that all pressure sensors are located on the surface of a virtual cone co-axial with the jet, so that their radial locations are a function of their axial locations.

The individual pressure signals from the sensors in the azimuthal arrays are denoted as $P^a : \mathbb{T}\times\mathbb{R}\times\mathcal{X}_p^a \to \mathbb{R},\ P^a : (\theta,t;x) \mapsto \mathbb{R}$; recall that this represents the normalized pressure per Sec. II.A. As before, the mean and fluctuating pressure are defined as $\overline{P}^a(x) := E\left\{(1/2\pi)\int_{-\pi}^{\pi} P^a(\theta,t;x)\mathrm{d}\theta\right\}$ and $p^a(\theta,t;x) = P^a(\theta,t;x) - \overline{P}^a(x)$, respectively. Similarly, the pressure signals on the linear array are denoted as $P^l : \mathbb{R}\times\mathcal{X}_p^l \to \mathbb{R},\ P^l : (t;x) \mapsto \mathbb{R}$. The corresponding time-mean and fluctuating quantities are respectively $\overline{P}^l(x) := E\left\{P^l(t;x)\right\}$, and $p^l(t;x)$. The azimuthal Fourier transform of the pressure signals from the azimuthal arrays are defined in the usual manner: $p^a(\theta,t;x) \xrightarrow{\mathcal{F}_m} \hat{p}^a(t;x,m)$. Of course, no such transformation is possible for $p^l(t;x)$.

The formulation of the SLSE is quite similar for the three cases that are studied here (all are performed in the azimuthal Fourier domain): (*a*) the original technique for estimating the velocity field $\hat{\mathbf{v}}(r,t;x,m)$, (*b*) the complementary technique for estimating the scalar POD modal coefficients $\hat{\gamma}_i^{(n)}(t;x,m),\ \forall i \in \{x,r,\theta\}$, and (*c*) the complementary technique for estimating the vector POD modal coefficients $\hat{\beta}^{(n)}(t;x,m)$. We will show the equations for case (*b*), as those for the other two cases can be readily deduced from it.

The finite temporal Fourier transforms of the pressure signals are defined as:[55]

$$\check{p}^a(x,m,f) := \int_{t=t_0-T/2}^{t_0+T/2} \hat{p}^a(t;x,m)\mathrm{e}^{-2\pi\mathrm{i}ft}\mathrm{d}t, \quad \check{p}^l(x,f) := \int_{t=t_0-T/2}^{t_0+T/2} p^l(t;x)\mathrm{e}^{-2\pi\mathrm{i}ft}\mathrm{d}t, \tag{15}$$

where, f is the temporal frequency, and t_0 locates the mid-point of a time-series of length T.

Let us denote the temporal Fourier transform of $\hat{\gamma}_i^{(n)}(t;x',m)$ by $\check{\gamma}_i^{(n)}(x',m,f)$, where $x' \in \mathcal{X}_v$ is the location of the cross-stream slice. Generalizing the formulation of Ref. 53, the latter is estimated as

$$\check{\gamma}_i^{(n)}(x',m,f) \approx \mathcal{L}_{\gamma_i}^{a,(n)}(x_k,x',m,f)\check{p}^a(x_k,m,f) + \mathcal{L}_{\gamma_i}^{l,(n)}(x_q,x',m,f)\check{p}^l(x_q,f), \quad \forall i \in \{x,r,\theta\}. \tag{16}$$

Einstein's summing convention is to be followed for the indices k and q, but not for m and f.[53] The standard least-squares technique gives the following set of linear equations for computing the estimation coefficients $\mathcal{L}^a$ and $\mathcal{L}^l$:

$$S_{pp}^{aa}(x_j,x_k,m,f)\mathcal{L}_{\gamma_i}^{a,(n)}(x_k,x',m,f)+S_{pp}^{al}(x_j,x_k,m,f)\mathcal{L}_{\gamma_i}^{l,(n)}(x_k,x',m,f)=S_{p\gamma_i}^{a,(n)}(x_j,x',m,f) \tag{17a}$$

$$S_{pp}^{al*}(x_k,x_j,m,f)\mathcal{L}_{\gamma_i}^{a,(n)}(x_k,x',m,f)+S_{pp}^{ll}(x_j,x_k,f)\mathcal{L}_{\gamma_i}^{l,(n)}(x_k,x',m,f)=S_{p\gamma_i}^{l,(n)}(x_j,x',m,f). \tag{17b}$$

Here, the cross-spectral tensors of pressure are defined as

$$S_{pp}^{aa}(x_j,x_k,m,f):=\lim_{T\to\infty}\frac{1}{T}E\left\{\check{p}^{a*}(x_j,m,f)\check{p}^{a}(x_k,m,f)\right\} \tag{18a}$$

$$S_{pp}^{al}(x_j,x_k,m,f):=\lim_{T\to\infty}\frac{1}{T}E\left\{\check{p}^{a*}(x_j,m,f)\check{p}^{l}(x_k,f)\right\} \tag{18b}$$

$$S_{pp}^{ll}(x_j,x_k,f):=\lim_{T\to\infty}\frac{1}{T}E\left\{\check{p}^{l*}(x_j,f)\check{p}^{l}(x_k,f)\right\}. \tag{18c}$$

The expectation operator is the un-weighted average over different independent blocks of size T. Keeping in mind the experimental realities, the cross-spectral tensors between pressure and the modal coefficients are computed in a different, but equivalent, manner:[55]

$$S_{p\gamma_i}^{a,(n)}(x,x',m,f):=\int_{\tau=-\infty}^{\infty}E\left\{\hat{p}^{a*}(t-\tau;x,m)\hat{\gamma}_i^{(n)}(t;x',m)\right\}\mathrm{e}^{-2\pi\mathrm{i}f\tau}\mathrm{d}\tau \tag{19a}$$

$$S_{p\gamma_i}^{l,(n)}(x,x',m,f):=\int_{\tau=-\infty}^{\infty}E\left\{\hat{p}^{l*}(t-\tau;x)\hat{\gamma}_i^{(n)}(t;x',m)\right\}\mathrm{e}^{-2\pi\mathrm{i}f\tau}\mathrm{d}\tau. \tag{19b}$$

The axisymmetry of the flow can be used to prove that cross-spectral tensors and the estimation coefficients are Hermitian functions of the temporal frequency f; these were enforced in our implementation.

Once $\check{\gamma}_i^{(n)}(x',m,f)$ is estimated in the temporal frequency domain, inverse Fourier transform yields the estimate of $\hat{\gamma}_i^{(n)}(t;x',m)$ in the time domain. This estimate is most accurate for $t=t_0$, the center of the original pressure time-series. So, it is best to perform steps (15), (16), and the inverse transform, separately for each time instant t_0 for which the velocity field is desired. Recall that the SLSE is intended for off-line implementation so that accuracy considerations can be allowed to trump computational efficiency. The actual velocity field is reconstructed using (13).

In summary, using the time-resolved pressure record, one can estimate the velocity fields on each of the cross-stream slices in $\mathcal{X}_v$ simultaneously, for any desired time instant. This then constitutes a database of estimated realizations of the 3-component velocity field on a 3D volumetric region of the jet mixing layer.[53]

In Ref. 53, experimental expediency dictated that the cross-stream PIV slices could not be taken on an axial grid that was fine enough for the reliable computation of the required spatial derivatives. Cubic spline interpolation was used to solve this problem.[64,65] The same method is adopted here to render the database amenable for the subsequent GP. Along with the fluctuating velocity field, the GP also requires the spatially-resolved mean velocity field. This can be reconstructed by again using cubic spline interpolation to estimate the mean velocity on a grid of desired axial resolution from the measured mean velocities on the original coarse grid of cross-stream slices.

II.D. 2D Proper Orthogonal Decomposition on 3D Velocity Database

In the foregoing discussions, various methods of obtaining a spatially-resolved 3D velocity database have been detailed. In the current work, one other possibility is of course to use the DNS database directly. All these fields are spatially resolved in the axial direction, unlike the velocity field described in Sec. II.B; hence the following notation is introduced.

Recall the implicit normalizations described in Sec. II.A. Now, suppose that the three components of velocity are known in a 3D cylindrical domain containing the mixing layer of the axisymmetric jet at several time instants (see Fig. 1). Then the streamwise velocity component is denoted as $U_x:[X_1,X_2]\times[0,R]\times\mathbb{T}\times\mathbb{R}\to\mathbb{R}$, $U_x:(x,r,\theta,t)\mapsto\mathbb{R}$. Here, X_1 and X_2 denote the beginning and end of the streamwise domain; note that $[X_1,X_2]$ should be covered by $\mathcal{X}_v$ for the experimental procedure. The remaining notations have been introduced before. Similarly, the radial and azimuthal components of the velocity field are denoted as U_r and U_θ, respectively. The flow velocity vector is then defined as $\mathbf{U}:=(U_x,U_r,U_\theta)^T\in\mathbb{R}^3$. As

before, the mean and fluctuating velocity fields are defined as $\overline{\mathbf{U}}(x,r) := E\left\{(1/2\pi)\int_{-\pi}^{\pi}\mathbf{U}(x,r,\theta,t)\mathrm{d}\theta\right\}$ and $\mathbf{u}(x,r,\theta,t) := \mathbf{U}(x,r,\theta,t) - \overline{\mathbf{U}}(x,r)$, respectively. The axial, radial, and azimuthal components of the fluctuating field are respectively u_x, u_r, and u_θ. The azimuthal Fourier transform of the fluctuating velocity field is defined as $\mathbf{u}(x,r,\theta,t) \xrightarrow{\mathcal{F}_m} \hat{\mathbf{u}}(x,r,t;m)$. Note that this is the quantity that is actually reconstructed in Sec. II.C.

The formulation of the 2D POD is very similar to the previous description of the 1D POD method. In the present case also, one transforms the velocity to the Fourier azimuthal domain (to account for the homogeneity of this direction), before applying the POD to the inhomogeneous axial and radial directions. The basic symmetry condition established in (1) still holds with the obvious modification, so that all the symmetries derived thereof also carry over. These similarities in the procedures allow us to avoid repeating the entire formulation. The fundamental inner product involved is presented below; however, the remaining equations are given for later reference and could actually be readily deduced from the 1D problem description in Sec. II.B. Only the vector POD is pursued here since it produces superior results to the scalar version in the subsequent GP.[43]

The inner product is defined in the azimuthal Fourier transform domain to relate it to the TKE. The definition is

$$\left\langle \hat{\mathbf{u}}^{(1)} \ , \ \hat{\mathbf{u}}^{(2)} \right\rangle := \int_{X_1}^{X_2}\int_0^R \hat{\mathbf{u}}^{(2)*}\hat{\mathbf{u}}^{(1)} r\mathrm{d}r\mathrm{d}x, \tag{20}$$

where $\hat{\mathbf{u}}^{(1)}$ and $\hat{\mathbf{u}}^{(2)}$ denote two arbitrary fields. With this, the vector POD problem can be shown to be

$$\int_{X_1}^{X_2}\int_0^R E\left\{\hat{u}_i(x,r,t;m)\hat{u}_j^*(x',r',t;m)\right\}\hat{\Phi}_j^{(n)}(x',r';m)r'\mathrm{d}r'\mathrm{d}x' = \Lambda^{(n)}(m)\hat{\Phi}_i^{(n)}(x,r;m),\ \forall i\in\{x,r,\theta\}. \tag{21}$$

The nth POD eigenvalue and eigenfunction Λ and $\hat{\mathbf{\Phi}}$ are parameterized by the azimuthal mode m, and the latter is also a function of the axial and radial location.

As an aside, the POD problem can be solved by the original method[32] or the snapshot method[52] depending on how the total number of points on the 2D grid compares to the number of realizations needed for statistical convergence. In the snapshot method, one does not explicitly use the kernel shown in (21), so that its symmetries cannot be applied directly. Instead, an option is to extend the database of realizations with the co-velocity field as described before (use (1), *mutatis mutandis*).[52] Of course, this doubles the number of realizations, thereby making the snapshot method less attractive.

Once the eigenfunctions are obtained, a low-dimensional reconstruction of the velocity field (in the Fourier azimuthal domain) can be obtained using only the first $N_{n,2}$ eigenfunctions:

$$\hat{\mathbf{u}}(x,r,t;m) \approx \sum_{n=1}^{N_{n,2}} \hat{\alpha}^{(n)}(t;m)\hat{\mathbf{\Phi}}^{(n)}(x,r;m), \tag{22}$$

with the modal coefficients computed from

$$\hat{\alpha}^{(n)}(t;m) = \left\langle \hat{\mathbf{u}}(x,r,t;m) \ , \ \hat{\mathbf{\Phi}}^{(n)}(x,r;m)\right\rangle. \tag{23}$$

As for the 1D POD, since $\hat{\mathbf{u}}$ and $\hat{\mathbf{\Phi}}$ are Hermitian in m, so is $\hat{\alpha}$. The subsequent GP models the dynamics of the modal coefficients, and their Hermitian-symmetric nature deduced above means that the model only need consider the non-negative azimuthal modes. This reduces the size of the ROM by almost a half.

II.E. Galerkin Projection

In Sec. II.B.3, we have remarked that the *incompressible* Navier-Stokes equations are most feasibly approximated using experimental data. The non-dimensionalized incompressible Navier-Stokes equations in cylindrical coordinates are[66]

$$\begin{aligned}\frac{\partial U_i}{\partial t} &= -(\mathbf{U}\cdot\nabla)U_i + \frac{U_\theta^2}{r}\delta_{ir} - \frac{U_r U_\theta}{r}\delta_{i\theta} - \nabla_i P \\ &\quad + \frac{1}{Re}\left\{\nabla^2 U_i + \left(-\frac{U_r}{r^2} - \frac{2}{r^2}\frac{\partial U_\theta}{\partial\theta}\right)\delta_{ir} + \left(-\frac{U_\theta}{r^2} + \frac{2}{r^2}\frac{\partial U_r}{\partial\theta}\right)\delta_{i\theta}\right\}, \quad i\in\{x,r,\theta\}.\end{aligned} \tag{24}$$

Here $\mathbf{U}$ is the velocity vector defined in Sec. II.D, P is the static pressure field (normalized per Sec. II.A), δ is the Kronecker delta, and ∇ and ∇^2 are respectively the gradient and Laplacian operators in cylindrical coordinates.

The POD procedure in Sec. II.D has produced an orthonormal basis for the velocity *fluctuations*; thus, before the GP is undertaken, the Reynolds decomposition must be applied to the Navier-Stokes equations. A dichotomy exists in the ROM literature regarding the appropriate mean field representation. One group has used a steady mean field derived from empirical data by ensemble-averaging as well as averaging over any homogenous direction, if applicable.[42,45,67–69] Another group of researchers have used simplifying assumptions to adopt a slowly time-varying mean field averaged over all homogenous directions, followed by its representation in terms of the Reynolds stresses.[22,23,38,39,41] For the axisymmetric jet, these assumptions were *not* borne out by our investigations using the DNS database, thereby prompting the adoption of a steady empirical mean field.

Applying the ensemble- and azimuthal-averaging to the Navier-Stokes equation (24) and subtracting the result from the original, one can readily obtain the dynamics of the velocity fluctuations as

$$\begin{aligned}\frac{\partial u_i}{\partial t} = &-\overline{U}_x\frac{\partial u_i}{\partial x} - \overline{U}_r\frac{\partial u_i}{\partial r} - u_x\frac{\partial \overline{U}_x}{\partial x}\delta_{ix} - u_r\frac{\partial \overline{U}_x}{\partial r}\delta_{ix} - u_x\frac{\partial \overline{U}_r}{\partial x}\delta_{ir} - u_r\frac{\partial \overline{U}_r}{\partial r}\delta_{ir} - \frac{\overline{U}_r u_\theta}{r}\delta_{i\theta}\\ &- (u\cdot\nabla)u_i + \overline{(u\cdot\nabla)u_i} + \frac{u_\theta^2 - \overline{u_\theta^2}}{r}\delta_{ir} - \frac{u_r u_\theta - \overline{u_r u_\theta}}{r}\delta_{i\theta} - \nabla_i p\\ &+ \frac{1}{Re}\left\{\nabla^2 u_i + \left(-\frac{u_r}{r^2} - \frac{2}{r^2}\frac{\partial u_\theta}{\partial\theta}\right)\delta_{ir} + \left(-\frac{u_\theta}{r^2} + \frac{2}{r^2}\frac{\partial u_r}{\partial\theta}\right)\delta_{i\theta}\right\}, \quad i\in\{x,r,\theta\}. \end{aligned} \tag{25}$$

Here, p is the pressure fluctuation; its azimuthal Fourier transform is defined as $p(x,r,\theta,t) \xrightarrow{\mathcal{F}_m} \hat{p}(x,r,t;m)$.

The subsequent steps in the GP are standard: application of an azimuthal Fourier transform to the equations, followed by a projection on to the POD basis functions $\hat{\mathbf{\Phi}}^{(n)}(x,r;m)$.[29] Assume that the velocity field is expanded using the first $N_{n,2}$ POD modes, and azimuthal modes $m=0$ to $m=N_m$. Then the resulting set of ODEs can be written as

$$\begin{aligned}\dot{\hat{\alpha}}^{(n)}(m) = &\sum_{j=1}^{N_{n,2}}\left\{\left(\frac{1}{Re} + \frac{\delta_{nj}}{Re_T^{(n)}(m)}\right)L_{nj}(m) + K_{nj}(m)\right\}\hat{\alpha}^{(j)}(m) - \left|\int_0^R \hat{p}(x,r,t;m)\hat{\Phi}_x^{(n)*}(x,r;m)r\mathrm{d}r\right|_{x=X_1}^{X_2}\\ &+ (1-\delta_{m0})\sum_{m'=m-N_m}^{N_m}\sum_{j,l=1}^{N_{n,2}} Q_{njl}(m,m')\times\hat{\alpha}^{(j)}(m')\hat{\alpha}^{(l)}(m-m'), \quad \forall n\in[1,N_{n,2}],\ \forall m\in[0,N_m]. \end{aligned} \tag{26}$$

The expressions for the coefficients appear in Appendix A.

For the assumed incompressible flow under consideration, the pressure term reduces to a surface integral over the boundary of the POD domain.[42] Moreover, owing to the ceasing of velocity fluctuations at the outer radius of the POD domain, the eigenfunctions themselves vanish at this boundary too. Therefore, one obtains the form shown above wherein the pressure needs to be evaluated at the inflow and outflow cross-stream slices only. Even in this simplified form, the term cannot be retained in the ROM since the requisite pressure information cannot be obtained from experiments. In previous applications to similar unbounded flows,[42,68] the term has been assumed to vanish altogether. Using the DNS database, we verified that indeed no appreciable inaccuracy is introduced by neglecting the pressure term for the unforced flow. The pressure term is implicitly neglected for the simulation results presented subsequently. We note here that in Ref. 70, it was shown that for the cylinder wake flow simulations, it is most appropriate to retain the pressure term, and to solve for it in parallel using the pressure Poisson equation.

The eigenfunction-basis of the velocity is truncated in both the Fourier space as well as the POD space, keeping only the most energetic modes. The neglected modes have low energy and typically correspond to the smaller-scales of turbulence; this makes them important for dissipation. Thus neglecting these modes generally has the effect of making the ROM overly energetic. It is usual to model the effect of these neglected modes using an eddy-viscosity representation. In the past, some researchers have incorporated a global eddy viscosity and treated it as a bifurcation parameter.[38,39,41] Others have computed empirical values of modal eddy viscosities by balancing energy or momentum.[45,71,72] Both these strategies amount in adding linear terms to the ROM, but the latter strategy gives more flexibility. Here, we follow the empirical energy balance route to modeling the eddy viscosity,[71] because it was effective in the cavity tone control model developed

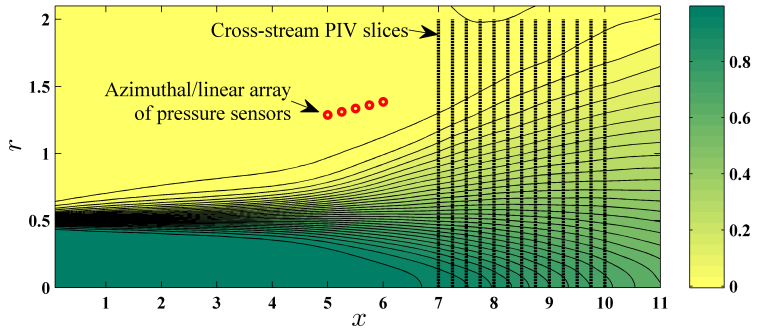

Figure 3. Contour plot of mean axial velocity from the DNS database.

in our laboratory.[45] In particular, the non-negative modal eddy Reynolds number $Re_T^{(n)}(m)$ is computed by requiring that the modal kinetic energy be steady in the ensemble-average over the database of realizations. Neglecting the pressure term, this leads to[71]

$$\frac{1}{Re_T^{(n)}(m)} = \max\left[0, -\frac{1}{Re} - \frac{1}{L_{nn}(m)\Lambda^{(n)}(m)}\left\{K_{nn}(m)\Lambda^{(n)}(m) + (1-\delta_{m0})\sum_{m'=m-N_m}^{N_m}\sum_{j,l=1}^{N_{n,2}} Q_{njl}(m,m')\right.\right.$$
$$\left.\left.\times E\left\{\Re\left(\hat{\alpha}^{(n)*}(m)\hat{\alpha}^{(j)}(m')\hat{\alpha}^{(l)}(m-m')\right)\right\}\right\}\right], \quad \forall n \in [1, N_{n,2}],\ \forall m \in [0, N_m]. \tag{27}$$

III. Results and Discussion

III.A. Preliminaries

The details of the direct numerical simulation database are available in Ref. 49; here we only highlight the most pertinent aspects. The cylindrical computational grid has 80 uniformly spaced azimuthal grid-points. For ease of implementation, the originally non-uniform rectangular $x-r$ grid is linearly interpolated hereby to a uniform square grid with a spacing of 0.0625 (in jet diameter coordinates). The data is saved at 2316 consecutive time instants with uniform separation of 0.071 (in t^+ coordinates).

The ROM is developed for controlling the large-scale structures in the turbulent jet mixing layer near the end of the potential core. If the model domain is too short to accommodate the typical large-scale structures in their entirety, then their dynamics cannot be modeled correctly.[42] The constraint at the other extreme is the necessity for the near-field pressure at the upstream location to be well-correlated to the velocity field on the cross-stream slice at the most downstream location for the success of the SLSE procedure. The low-Re simulated jet remains laminar for a significant length,[49] whereas the high-Re experimental jet is turbulent at its exit.[13] For the present exercise to be of use in designing later experiments, the modeling should be performed using data from a domain of the simulated jet mixing layer that is turbulent.

A contour plot of the mean axial velocity is shown in Fig. 3. The transition from laminar to turbulent flow is difficult to pin-point; however, a difference in the jet-spreading behavior is noted at $x \approx 5$. Practical considerations would prevent the placement of pressure sensors too far downstream in actual applications; this constrains their feasible axial locations. The need to obtain a hydrodynamic signature dictates the radial location of the sensors.[53,73,74] Five conceptual sensors are placed in a uniform linear array from $x = 5$ to 6, making an angle of 5.6^o with the jet axis, with the most upstream sensor located at $r = 1.29$ (see Fig. 3). Alternatively, any or all of them may be replaced by azimuthal arrays of 80 sensors (of the form shown in Fig. 1), corresponding to the DNS grid. Following the discussion above, conceptual cross-stream slices of the flow were chosen in the range $x = 7$ to 10 at intervals of 0.25 to perform the 1D slice-POD (see Fig. 3). The radial extent of the slice-POD domain was $R = 2$.

III.B. Results of 3D Velocity Field Reconstruction using SLSE

The application of 1D slice-POD to the axisymmetric jet mixing layer is standard, and the results have been published in Ref. 37. Here, we will directly proceed to a discussion of the accuracy of reconstruction

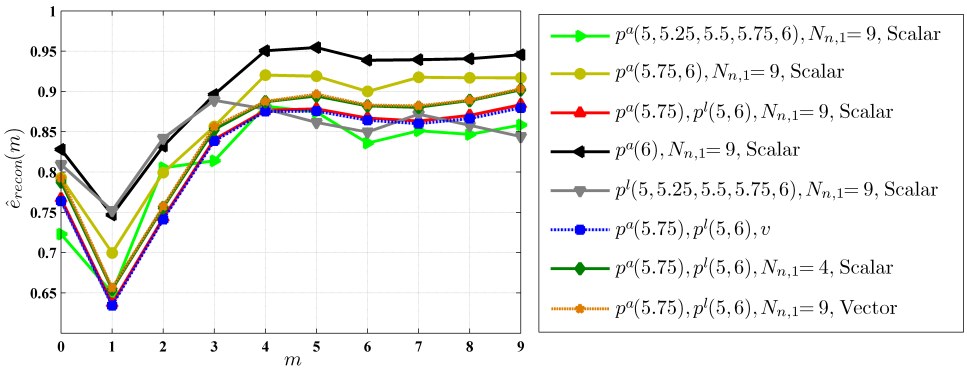

Figure 4. The reconstruction error for various routes to stochastic estimation.

of the 3D velocity field database using SLSE. The details of the implementation of the SLSE, as well as the qualitative nature of the results follow Ref. 53; and are not repeated here. We only mention that the finite time Fourier transforms were implemented with T corresponding to 400 samples, and overlaps of 300 samples. The DNS database provides an opportunity to assess the performance of several optional routes of the SLSE, and this will be pursued here. The cubic spline interpolation is kept out of this exercise for the time-being, to focus on the SLSE alone.

Using any of the methods described previously, one obtains the reconstructed fluctuating velocity field denoted by $\tilde{\hat{\mathbf{v}}}(r,t;x,m)$. The actual fluctuating velocity field $\hat{\mathbf{v}}(r,t;x,m)$ at these axial locations is also known for the same time instant t. Thus, we define the following reconstruction error metric:

$$\hat{e}_{recon}(m) := \frac{\sum_{x\in\mathcal{X}_v} E\left\{\left|\left|\tilde{\hat{\mathbf{v}}}(r,t;x,m) - \hat{\mathbf{v}}(r,t;x,m)\right|\right|^2\right\}}{\sum_{x\in\mathcal{X}_v} E\left\{||\hat{\mathbf{v}}(r,t;x,m)||^2\right\}}. \tag{28}$$

The above norm is induced from the inner-product defined in (6).

The comparison of the reconstruction errors is presented in Fig. 4. Here p^a and p^l signify the use of the azimuthal and linear arrays, respectively; their x locations appear in parentheses. The symbol v denotes the application of SLSE to the velocity field. Otherwise, the complementary SLSE is employed to estimate the first $N_{n,1}$ POD modal coefficients as noted. 'Scalar' and 'vector' respectively indicate the type of POD.

Although the errors are quite large in general, it will be shown that the reconstructed database is still useful for the subsequent 2D POD. Using more pressure information does not always result in improved accuracy of reconstruction, since the estimation may become over-optimized for the reference data. Thus, for some azimuthal modes, using all 5 azimuthal arrays is seen to result in more errors than using 1 or 2 arrays only. Moreover, 5 azimuthal arrays would be prohibitively expensive and complicated to implement. The best arrangement involving one azimuthal array and any number of sensors from the linear array is $p^a(5.75), p^l(5,6)$. This is seen to produce better results when compared to the best case of using two azimuthal arrays, $p^a(5.75,6)$. A single azimuthal array was used in Ref. 53; the best case of this situation here is $p^a(6)$, and it is seen to perform quite poorly. Using just the linear array is seen to produce better results than using it in conjunction with an azimuthal array, but only for some higher azimuthal modes. The complementary SLSE using the estimated scalar 1D slice POD coefficients is more accurate compared to the vector POD. This is to be expected, since the latter aggregates the information provided by the pressure sensors. Adding more POD modes improves the fidelity, although the direct reconstruction of the velocity field (avoiding the complementary technique) performs similar to the case of $N_{n,1} = 9$.

In the remaining article, we will focus on the database reconstructed using the scalar 1D POD modal coefficients with $N_{n,1} = 9$ and the pressure sensor configuration selected as $p^a(5.75), p^l(5,6)$. This will be referred to as the "chosen" reconstructed database. Before proceeding to the next step, we implement the cubic spline interpolation that was held in abeyance for the above considerations.

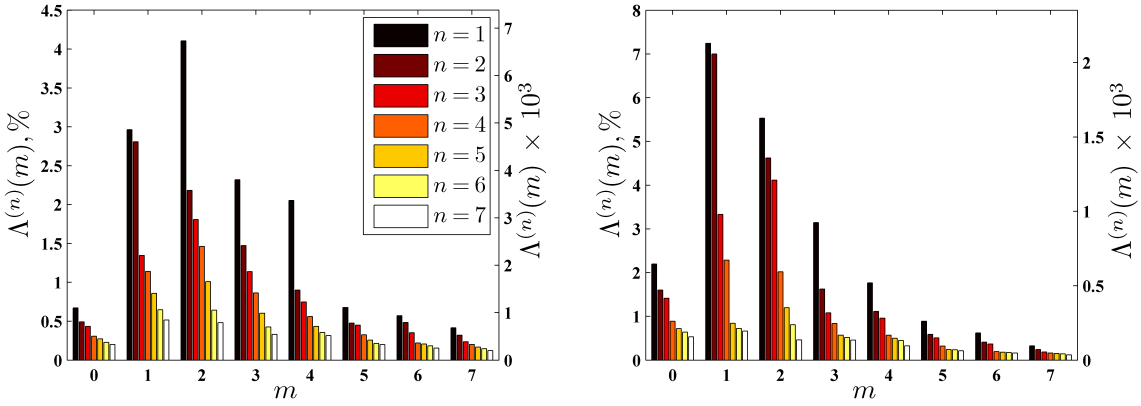

Figure 5. 2D POD eigenvalue spectra for (a) the original DNS database, and (b) the reconstructed database chosen in Sec. III.B.

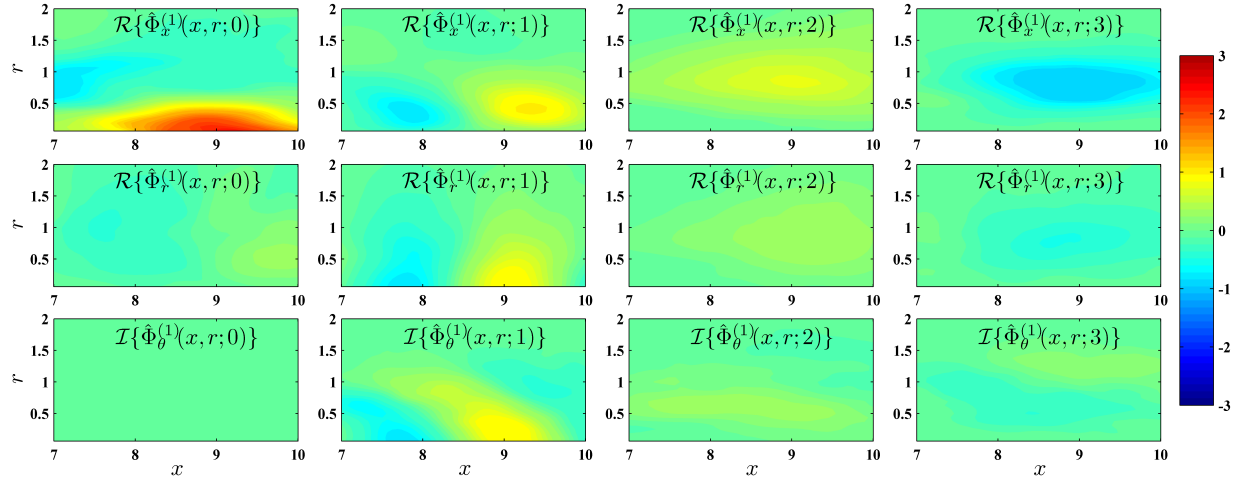

Figure 6. 2D POD eigenfunctions educed from the original DNS database.

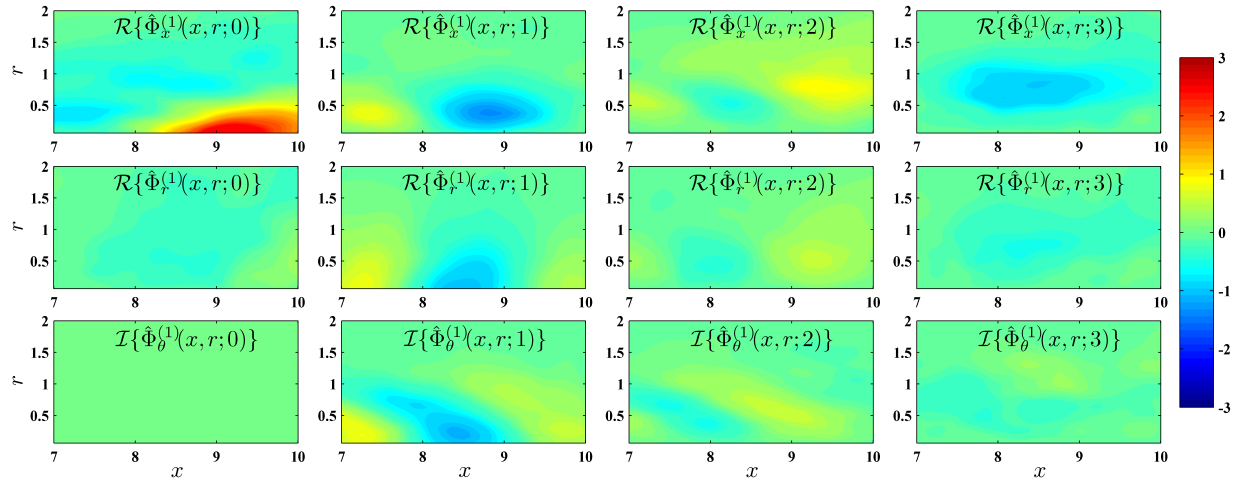

Figure 7. 2D POD eigenfunctions educed from the reconstructed database chosen in Sec. III.B.

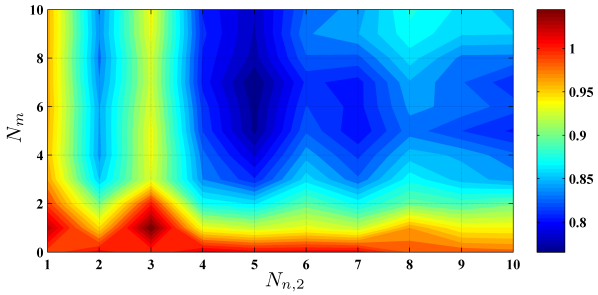

Figure 8. Simulation error e_{sim} for ROMs built from the original DNS database for various choices of the cutoff.

III.C. Results of 2D POD on 3D Velocity Database

The eigenvalues obtained from the application of the 2D vector POD discussed in Sec. II.D are presented in Fig. 5 as a percentage of the respective total energy captured, as well in terms of their absolute values. Since all the energy is not captured in the reconstructed database, the actual percentages are unimportant, and one should focus on the relative energies within each sub-figure. With this caveat, it is apparent that the reconstruction shows some discrepancies with an over-prediction of $m = 1$, and under-prediction of $m = 4$. The near equality of the 1st and 2nd POD modes for $m = 1$ in both cases is indicative of an approximate periodic behavior in this mode.[29]

Figs. 6 and 7 present some representative eigenfunctions corresponding to the two databases discussed in Fig. 5. Following the 2D POD counterpart of (10), only the non-trivial components of the first POD eigenfunctions are shown for azimuthal modes 0 through 3. In spite of the reconstruction errors seen in Fig. 4, we note the similarity of the POD eigenfunctions from the original DNS database and the chosen SLSE reconstruction in Figs. 6 and 7, respectively. One concludes that while the the reconstructed structures are weaker compared to the original, their shapes are captured well by the SLSE procedure. Discrepancies in the POD bases would not invalidate the subsequent GP; they would only result in a sub-optimal basis for the expansion, thereby introducing more inaccuracy for the same dimension of the ROM.

If a flow is incompressible, then each of its velocity realizations are solenoidal. The vector POD eigenfunctions for such a flow, being linear combinations of these realizations,[43] inherit the solenoidal property also. Thus one way of assessing the incompressibility assumption for the present flow is to determine how close $\hat{\mathbf{\Phi}}^{(n)}(x, r; m)$ is to being solenoidal. The following metric

$$\hat{e}_{sol}^{(n)}(m) := \frac{\displaystyle\int_{X_1}^{X_2}\int_0^R \left| \frac{\partial}{\partial x}\hat{\Phi}_x^{(n)}(x,r;m) + \frac{1}{r}\frac{\partial}{\partial r}\left\{r\hat{\Phi}_r^{(n)}(x,r;m)\right\} + \frac{m}{r}\hat{\Phi}_\theta^{(n)}(x,r;m)\right|^2 r\mathrm{d}r\mathrm{d}x}{\displaystyle\int_{X_1}^{X_2}\int_0^R \left[\left|\frac{\partial}{\partial x}\hat{\Phi}_x^{(n)}(x,r;m)\right|^2 + \left|\frac{1}{r}\frac{\partial}{\partial r}\left\{r\hat{\Phi}_r^{(n)}(x,r;m)\right\}\right|^2 + \left|\frac{m}{r}\hat{\Phi}_\theta^{(n)}(x,r;m)\right|^2\right] r\mathrm{d}r\mathrm{d}x}, \tag{29}$$

is evaluated for the eigenfunctions obtained from the original DNS database with n ranging from 1 to 10 and m ranging from 0 to 10. The maximum value of $\hat{e}_{sol}$ is found to be 0.7%, thereby lending support to the incompressibility assumption.

III.D. Results of Simulation of the ROM Obtained by Galerkin Projection

The first derivatives of the eigenfunctions and mean velocities appearing in the coefficients of the ROMs (see Appendix A) were computed using 6th-order accurate finite differences. The ROMs were simulated using MATLAB's `ode45`, which is a Runge-Kutta (4, 5) ODE solver with automatic step-size selection. Subsequently, the simulation results were linearly interpolated on the time axis of the DNS database for direct comparison. For control-purposes, the ROM needs to predict the flow over short periods, and we focused on a time horizon of $5t^+$ in all the results presented here. The initial condition was an arbitrary realization in the middle of the DNS save-record.

Let the simulated fluctuating velocity be denoted by $\tilde{\mathbf{u}}(x, r, \theta, t)$. The actual fluctuating velocity $\mathbf{u}(x, r, \theta, t)$

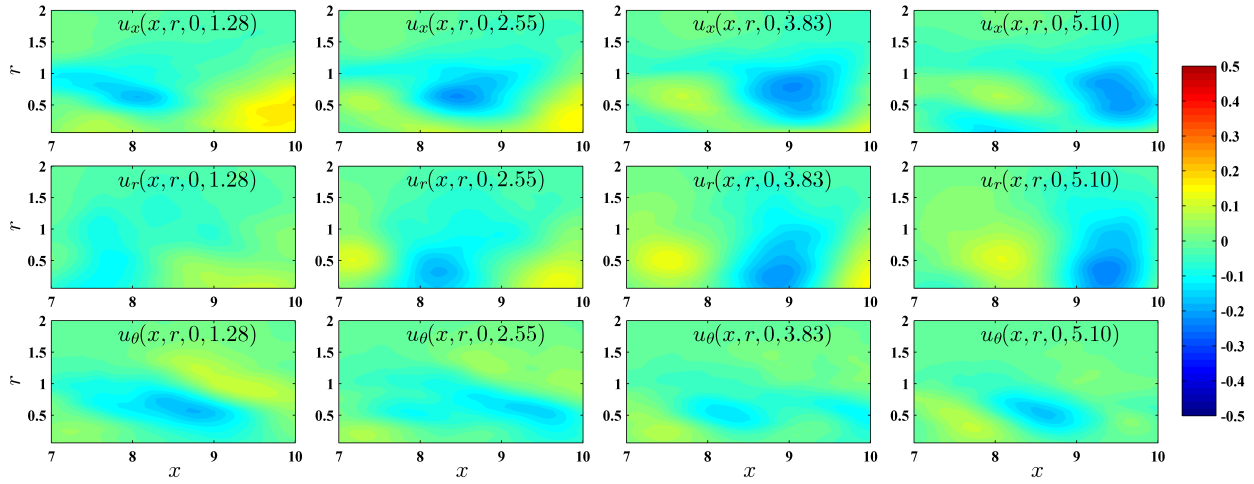

Figure 9. Evolution of a simulated 30D ROM educed from the original DNS database.

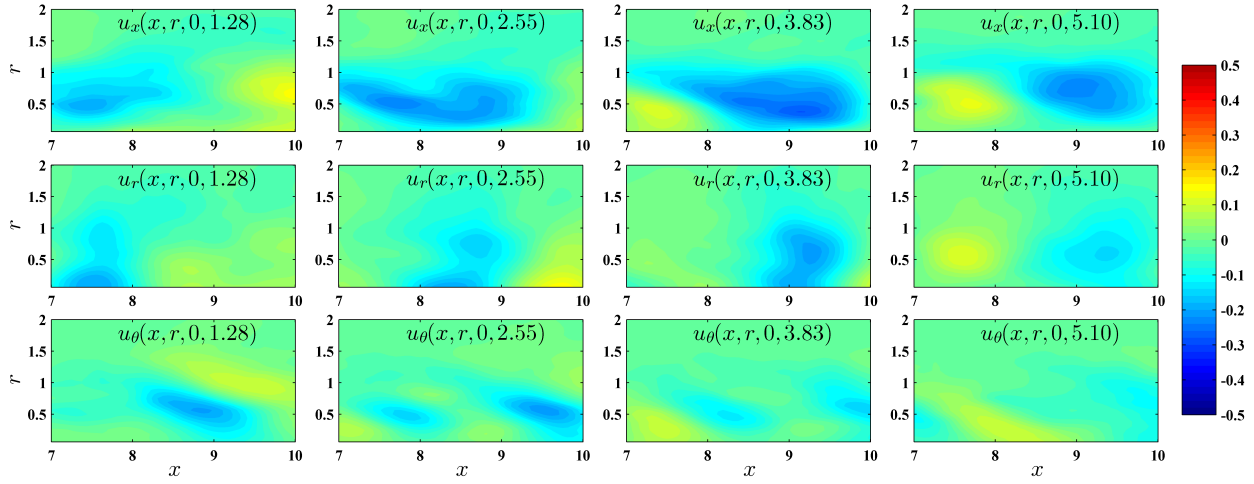

Figure 10. Original DNS realizations projected on the 30D basis used in Fig. 9, at matching time instants.

is also known at the same time instant t. A simulation error metric is defined as

$$e_{sim} := \frac{E\left\{\int_{-\pi}^{\pi}\int_{X_1}^{X_2}\int_0^R (\tilde{\mathbf{u}}-\mathbf{u})^*(\tilde{\mathbf{u}}-\mathbf{u})\, r\mathrm{d}r\mathrm{d}x\mathrm{d}\theta\right\}}{E\left\{\int_{-\pi}^{\pi}\int_{X_1}^{X_2}\int_0^R \mathbf{u}^*\mathbf{u} r\mathrm{d}r\mathrm{d}x\mathrm{d}\theta\right\}} = 1 + \frac{\sum_{m=-N_m}^{N_m}\sum_{n=1}^{N_{n,2}} E\left\{\left|\tilde{\hat{\alpha}}\right|^2 - 2\Re\left(\tilde{\hat{\alpha}}^*\hat{\alpha}\right)\right\}}{E\left\{\frac{1}{2\pi}\int_{-\pi}^{\pi}\int_{X_1}^{X_2}\int_0^R \mathbf{u}^*\mathbf{u} r\mathrm{d}r\mathrm{d}x\mathrm{d}\theta\right\}}. \quad (30)$$

The second expression follows from the orthonormality of the eigenfunction basis. Here, the POD modal coefficients $\hat{\alpha}^{(n)}(m)$ and $\tilde{\hat{\alpha}}^{(n)}(m)$ correspond to velocities $\mathbf{u}$ and $\tilde{\mathbf{u}}$, respectively.

Fig. 8 shows the simulation error evaluated for the ROMs developed using the original DNS database, for various choices of the cutoffs $N_{n,2}$ and N_m. The errors are quite large, demonstrating the inherent inaccuracies of low-dimensional modeling for this complicated flow. Including the largest number of modes does not always result in the most accurate model,[40,43,75] and this is observed here too. For real-time control, the dimension of the model must be kept at a minimum, and Fig. 8 suggests a choice of $N_{n,2} = 5$ and $N_m = 5$; for this $e_{sim} = 0.77$. These parameters define the 30-dimensional basis that is retained for the ROMs studied hereafter. Note that this basis captures 35% of the total energy of the flow.

The simulation error e_{sim} is a gross metric; to get a better intuition, we present some snapshots of the flow evolution from the ROM simulation in Fig. 9. The velocity fluctuations on the $\theta = 0$ plane are shown. The

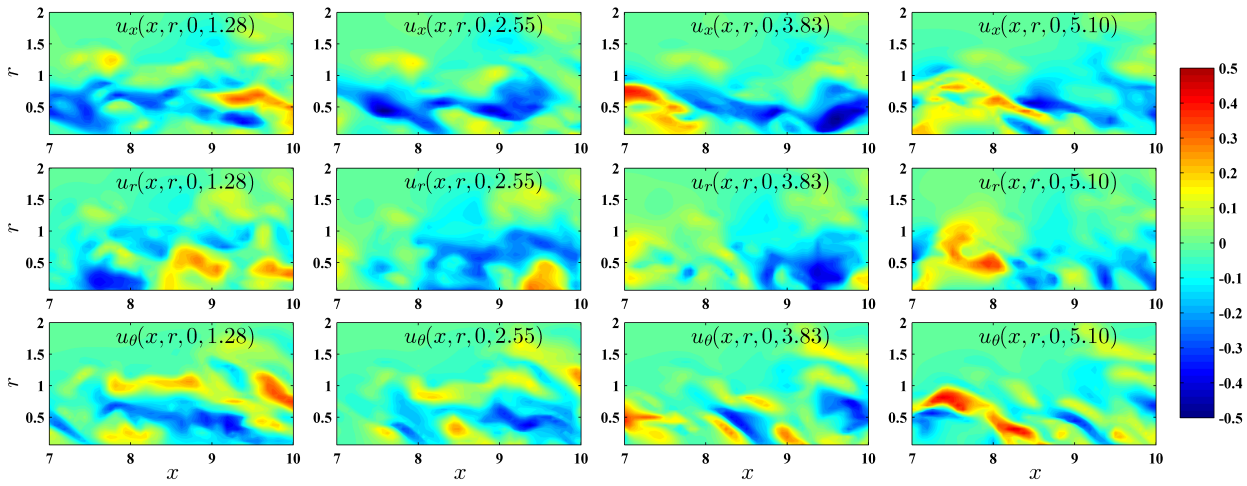

Figure 11. Original DNS realizations at time instants matching Fig. 9.

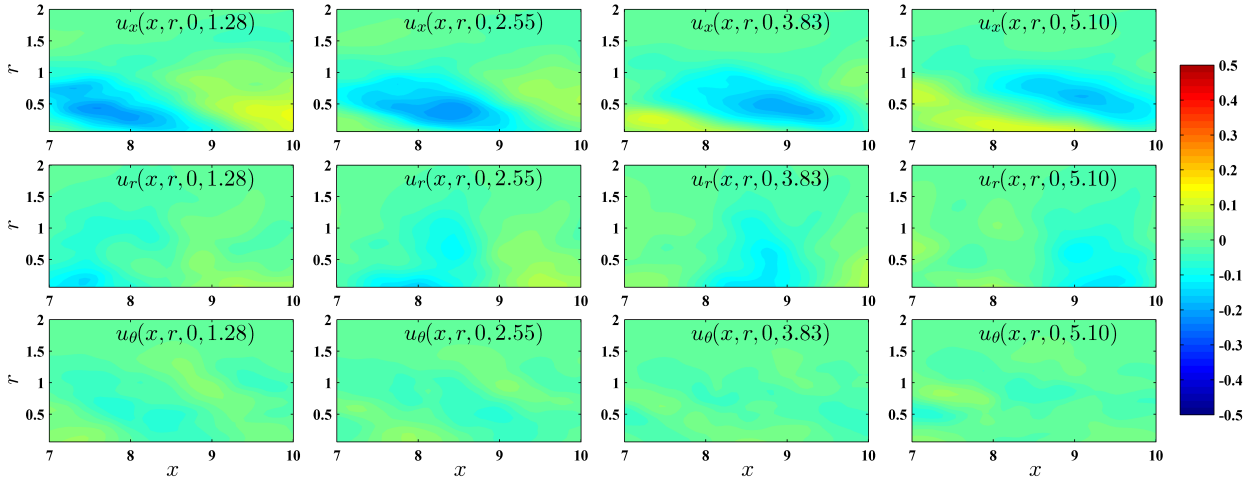

Figure 12. Evolution of a simulated 30D ROM educed from the reconstructed database chosen in Sec. III.B.

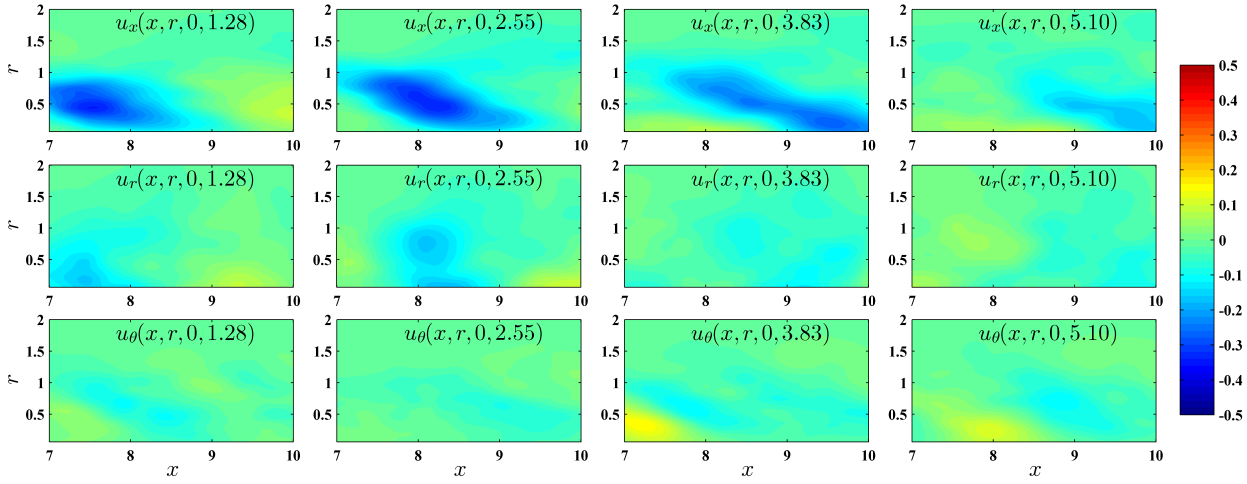

Figure 13. Reconstructed realizations projected on the 30D basis used in Fig. 12, at matching time instants.

time instants are measured from the initial condition chosen for generating Fig. 8. Fig. 9 is to be compared with Fig. 10 that shows the projection of the corresponding realizations of the original DNS database onto the same 30D eigenfunction basis. In Fig. 11 we also present the actual snapshots at the corresponding instants. As expected, the overall discrepancies are quite large, but most of the differences result from the use of a partial basis for the reconstruction. The different components of velocity are modeled with different accuracies with decreasing order being axial, radial, and azimuthal. The turbulent kinetic energies associated separately with the three components were also found to be ordered similarly for this database. Since the underlying vector POD is weighted towards the more energetic component, the perceived difference in modeling accuracy is to be expected. Overall, the low-dimensional dynamics of the flow are seen to be captured with good accuracy over the selected simulation time horizon.

An ROM was also derived by Galerkin projection onto the 2D POD basis educed from the reconstructed database chosen in Sec. III.B. The cutoffs were retained as $N_{n,2} = 5$ and $N_m = 5$ to define a new 30D basis. The initial time matched the previous simulation, and the corresponding reconstructed realization was projected onto the new 30D basis to obtain the set of initial POD modal coefficients. The evolution of this ROM is shown in Fig. 12; for this model $e_{sim} = 0.90$. For comparison, Fig. 13 shows the projection of the corresponding realizations onto the same basis. The shape and strength of the structures are seen to be quite alike in these two figure, thereby once again attesting to the fidelity of the Galerkin projection.

IV. Conclusion

The first step in model-based feedback flow control is the development of a reduced-order model of the unforced flow; this has been pursued here for an axisymmetric jet. An existing direct numerical simulation database of a Mach 0.9 low Reynolds number jet is used to guide the modeling, with an eye toward feasibility of later experimental implementation. The two phases of the modeling are (*a*) reconstructing a database of snapshots of the 3-component velocity field over the pertinent 3D domain of the jet mixing layer from experimentally accessible measurements, and (*b*) determining the dynamics of the most energetic structures in this domain.

For the first phase, we adopted the spectral linear stochastic estimation technique presented in Ref. 37, 53 that employs pressure measurements on an azimuthal array in the irrotational near-field of the jet. The estimation coefficients are determined from the cross-spectra between pressure measurements and low-dimensional representations of the velocity fields on individual cross-stream slices covering the axial domain of interest in the jet mixing layer. We showed here that the reconstruction fidelity is substantially improved by incorporating an additional linear array of pressure sensors in the near-field, at little extra cost. Additionally, we introduced a method to explicitly enforce the axisymmetry of the flow in the estimation.

For the second phase, proper orthogonal decomposition was used to educe a partial basis for the velocity field consisting of the most energetic structures. Subsequently, Galerkin projection of the incompressible Navier-Stokes equations onto this basis yielded a set of ordinary differential equations that govern their dynamics. To validate the procedure, a 30-dimensional basis was first derived from the original database. Simulations of the resulting model demonstrated that the evolution of the large-scale structures are well-captured. Finally, a basis of the same dimension was obtained from the database reconstructed in the first phase. Simulations of the resulting ROM showed that it may be acceptable for the purposes of feedback control.

Acknowledgments

The support of this research in part by the Air Force Office of Scientific Research through a joint grant program with Syracuse University and Clarkson University, with Dr. John Schmisseur as the program manager, is greatly appreciated. The authors would like to thank Dr. J. B. Freund for providing the DNS database, and Dr. Edgar Caraballo for insightful discussions.

Appendix A. Coefficients of the ROM

The expressions for the coefficients of the ROM presented in (26) are

$$L_{nj}(m) = \int_0^R \left[\left| \frac{\partial \hat{\Phi}_i^{(j)}(m)}{\partial x} \hat{\Phi}_i^{(n)*}(m) \right|_{X_1}^{X_2} - \int_{X_1}^{X_2} \frac{\partial \hat{\Phi}_i^{(j)}(m)}{\partial x} \frac{\partial \hat{\Phi}_i^{(n)*}(m)}{\partial x} \mathrm{d}x \right] r \mathrm{d}r$$
$$+ \int_{X_1}^{X_2} \left[\left| r \frac{\partial \hat{\Phi}_i^{(j)}(m)}{\partial r} \hat{\Phi}_i^{(n)*}(m) \right|_0^R - \int_0^R \frac{\partial \hat{\Phi}_i^{(j)}(m)}{\partial r} \frac{\partial \hat{\Phi}_i^{(n)*}(m)}{\partial r} r \mathrm{d}r \right] \mathrm{d}x$$
$$+ \int_{X_1}^{X_2} \int_0^R \left[-m^2 \hat{\Phi}_i^{(j)}(m) - \left\{ \hat{\Phi}_r^{(j)}(m) + 2\mathrm{i}m \hat{\Phi}_\theta^{(j)}(m) \right\} \delta_{ir} - \left\{ \hat{\Phi}_\theta^{(j)}(m) - 2\mathrm{i}m \hat{\Phi}_r^{(j)}(m) \right\} \delta_{i\theta} \right] \hat{\Phi}_i^{(n)*}(m) \frac{\mathrm{d}r\mathrm{d}x}{r}$$
$$K_{nj}(m) = \int_{X_1}^{X_2} \int_0^R \left[-\overline{U}_x \frac{\partial \hat{\Phi}_i^{(j)}(m)}{\partial x} - \overline{U}_r \frac{\partial \hat{\Phi}_i^{(j)}(m)}{\partial r} - \hat{\Phi}_x^{(j)}(m) \frac{\partial \overline{U}_x}{\partial x} \delta_{ix} - \hat{\Phi}_r^{(j)}(m) \frac{\partial \overline{U}_x}{\partial r} \delta_{ix} \right.$$
$$\left. - \hat{\Phi}_x^{(j)}(m) \frac{\partial \overline{U}_r}{\partial x} \delta_{ir} - \hat{\Phi}_r^{(j)}(m) \frac{\partial \overline{U}_r}{\partial r} \delta_{ir} - \frac{\overline{U}_r \hat{\Phi}_\theta^{(j)}(m)}{r} \delta_{i\theta} \right] \hat{\Phi}_i^{(n)*}(m) r \mathrm{d}r\mathrm{d}x$$
$$Q_{njl}(m, m') = \int_{X_1}^{X_2} \int_0^R \left[- \left\{ \hat{\Phi}_x^{(j)}(m') \frac{\partial}{\partial x} + \hat{\Phi}_r^{(j)}(m') \frac{\partial}{\partial r} + \frac{\mathrm{i}(m-m') \hat{\Phi}_\theta^{(j)}(m')}{r} \right\} \hat{\Phi}_i^{(l)}(m-m') \right.$$
$$\left. + \frac{\hat{\Phi}_\theta^{(j)}(m') \delta_{ir} - \hat{\Phi}_r^{(j)}(m') \delta_{i\theta}}{r} \hat{\Phi}_\theta^{(l)}(m-m') \right] \hat{\Phi}_i^{(n)*}(m) r \mathrm{d}r\mathrm{d}x.$$

In the above, the dependence of the eigenfunctions on x and r have been suppressed for notational convenience. For accuracy of numerical differentiation, the second-order spatial derivatives of the eigenfunctions have been transformed into first-order derivatives by integration-by-parts. The symmetries of the POD eigenfunctions established previously immediately lead to the conclusion that all the coefficients are purely real.

References

[1] Jordan, P. and Gervais, Y., "Subsonic jet aeroacoustics: associating experiment, modelling and simulation," *Experiments in Fluids*, Vol. 44, No. 1, 2008, pp. 1–21.

[2] Gutmark, E. J., Schadow, K. C., and Yu, K. H., "Mixing Enhancement in Supersonic Free Shear Flows," *Annu. Rev. Fluid Mech.*, Vol. 27, No. 1, 1995, pp. 375–417.

[3] Gad-el Hak, M., *Flow Control: Passive, Active, and Reactive Flow Management*, Cambridge Univ. Press, 2000.

[4] Aamo, O. M. and Krstić, M., *Flow Control by Feedback: Stabilization and Mixing*, Springer, 2003.

[5] Collis, S. S., Joslin, R. D., Seifert, A., and Theofilis, V., "Issues in active flow control: theory, control, simulation, and experiment," *Prog. Aerosp. Sci.*, Vol. 40, 2004, pp. 237–289.

[6] King, R., editor, *Active Flow Control - Papers Contributed to the Conference Active Flow Control 2006, Berlin, Germany, September 27 to 29, 2006*, Springer, 2007.

[7] Kim, J. and Bewley, T. R., "A Linear Systems Approach to Flow Control," *Annu. Rev. Fluid Mech.*, Vol. 39, 2007, pp. 383–417.

[8] Samimy, M., Kim, J.-H., Kastner, J., Adamovich, I., and Utkin, Y., "Active control of high-speed and high-Reynolds-number jets using plasma actuators," *Journal of Fluid Mechanics*, Vol. 578, 2007, pp. 305–330.

[9] Samimy, M., Kim, J.-H., Kastner, J., Adamovich, I., and Utkin, Y., "Active control of a Mach 0.9 jet for noise mitigation using plasma actuators," *AIAA Journal*, Vol. 45, No. 4, 2007, pp. 890–901.

[10] Utkin, Y. G., Keshav, S., Kim, J.-H., Kastner, J., Adamovich, I. V., and Samimy, M., "Development and use of localized arc filament plasma actuators for high-speed flow control," *Journal of Physics D: Applied Physics*, Vol. 40, No. 3, 2007, pp. 685–694.

[11] Kim, J.-H., Kastner, J., and Samimy, M., "Active Control of a High Reynolds Number Mach 0.9 Axisymmetric Jet," *AIAA Journal*, Vol. 47, No. 1, 2009, pp. 116–128.

[12] Kastner, J., Kim, J.-H., and Samimy, M., "A study of the correlation of large-scale structure dynamics and far-field radiated noise in an excited Mach 0.9 jet," *International Journal of Aeroacoustics*, Vol. 8, No. 3, 2009, pp. 231–259.

[13] Kearney-Fischer, M., Kim, J.-H., and Samimy, M., "Control of a High Reynolds Number Mach 0.9 Heated Jet Using Plasma Actuators," *Physics of Fluids*, Vol. 21, 2009, pp. 095101.

[14] Kearney-Fischer, M., Kim, J.-H., and Samimy, M., "Noise Control of a High Reynolds Number Mach 0.9 Heated Jet Using Plasma Actuators," *15th AIAA/CEAS Aeroacoustics Conference, AIAA Paper 2009-3188*, 2009.

[15]Krstić, M. and Wang, H.-H., "Stability of extremum seeking feedback for general nonlinear dynamic systems," *Automatica*, Vol. 36, No. 4, 2000, pp. 595–601.

[16]Henning, L., Becker, R., Feuerbach, G., Muminovic, R., King, R., Brunn, A., and Nitsche, W., "Extensions of adaptive slope-seeking for active flow control," *Proc. IMechE, Part I*, Vol. 222, No. 5, 2008, pp. 309–322.

[17]Kim, K., Kasnakoğlu, C., Serrani, A., and Samimy, M., "Extremum-Seeking Control of Subsonic Cavity Flow," *AIAA Journal*, Vol. 47, No. 1, 2009, pp. 195–205.

[18]Sinha, A., Kim, K., Kim, J.-H., Serrani, A., and Samimy, M., "Extremizing Feedback Control of a High-Speed and High Reynolds Number Jet," *to appear in AIAA Journal*, 2009.

[19]Pastoor, M., Henning, L., Noack, B. R., King, R., and Tadmor, G., "Feedback shear layer control for bluff body drag reduction," *Journal of Fluid Mechanics*, Vol. 608, 2008, pp. 161–196.

[20]Caraballo, E., Kasnakoğlu, C., Serrani, A., and Samimy, M., "Control Input Separation Methods for Reduced-Order Model-Based Feedback Flow Control," *AIAA Journal*, Vol. 46, No. 9, 2008, pp. 2306–2322.

[21]Tchieu, A. A., Kutay, A. T., Muse, J. A., Calise, A. J., and Leonard, A., "Validation of a Low-Order Model for Closed-Loop Flow Control Enabled Flight," *4th AIAA Flow Control Conference, AIAA Paper 2008-3863*, 2008.

[22]Noack, B. R., Afanasiev, K., Morzynski, M., Tadmor, G., and Thiele, F., "A hierarchy of low-dimensional models for the transient and post-transient cylinder wake," *Journal of Fluid Mechanics*, Vol. 497, 2003, pp. 335–363.

[23]Luchtenburg, D. M., Gunther, B., Noack, B., King, R., and Tadmor, G., "A generalized mean-field model of the natural and high-frequency actuated flow around a high-lift configuration," *Journal of Fluid Mechanics*, Vol. 623, 2009, pp. 283–316.

[24]Ljung, L., *System Identification - Theory for the user*, Prentice Hall, 1999.

[25]Perret, L., Collin, E., and Delville, J., "Polynomial identification of POD based low-order dynamical system," *Journal of Turbulence*, Vol. 7, No. 17, 2006, pp. 1–15.

[26]Henning, L., Pastoor, M., Noack, B. R., King, R., and Tadmor, G., "Feedback control applied to the bluff body wake," *Active Flow Control*, edited by R. King, Springer-Verlag, 2007, pp. 369–390.

[27]Efe, M. O., Debiasi, M., Yan, P., Ozbay, H., and Samimy, M., "Neural network-based modelling of subsonic cavity flows," *International Journal of Systems Science*, Vol. 39, No. 2, 2008, pp. 105–117.

[28]Siegel, S., Seidel, J., Fagley, C., Luchtenburg, D. M., Cohen, K., and McLaughlin, T., "Low-dimensional modelling of a transient cylinder wake using double proper orthogonal decomposition," *Journal of Fluid Mechanics*, Vol. 610, 2008, pp. 1–42.

[29]Holmes, P., Lumley, J., and Berkooz, G., *Turbulence, Coherent Structures, Dynamical Systems and Symmetry*, Cambridge University Press, 1996.

[30]Marion, M. and Temam, R., "Nonlinear Galerkin Methods," *SIAM J. Numer. Anal.*, Vol. 2005, No. 5, 1989, pp. 1139–1157.

[31]Debussche, A., Dubois, T., and Temam, R., "The Nonlinear Galerkin Method: A Multiscale Method Applied to the Simulation of Homogeneous Turbulent Flows," *Theoret. Comput. Fluid Dynamics*, Vol. 7, 1995, pp. 279–315.

[32]Lumley, J. L., "The Structure of Inhomogeneous Turbulent Flows," *Atm. Turb. and Radio Wave Prop.*, edited by A. M. Yaglom and V. I. Tatarsky, Nauka, Moscow, 1967, pp. 166–178.

[33]Glauser, M. N., Leib, S. J., and George, W. K., "Coherent structures in the axisymmetric jet mixing layer," *Proc. Fifth Int. Symp. Turbulent Shear Flows, Ithaca, USA*, 1985.

[34]Gamard, S., George, W. K., Jung, D., and Woodward, S., "Application of a slice proper orthogonal decomposition to the far field of an axisymmetric turbulent jet," *Physics of Fluids*, Vol. 14, No. 7, 2002, pp. 2515–2522.

[35]Jung, D. H., Gamard, S., and George, W. K., "Downstream evolution of the most energetic modes in a turbulent axisymmetric jet at high Reynolds number. Part 1. The near-field region," *Journal of Fluid Mechanics*, Vol. 514, 2004, pp. 173–204.

[36]Iqbal, M. O. and Thomas, F. O., "Coherent structure in a turbulent jet via a vector implementation of the proper orthogonal decomposition," *Journal of Fluid Mechanics*, Vol. 571, 2007, pp. 281–326.

[37]Tinney, C. E., Glauser, M. N., and Ukeiley, L. S., "Low-dimensional characteristics of a transonic jet. Part 1. Proper orthogonal decomposition," *Journal of Fluid Mechanics*, Vol. 612, 2008, pp. 107–141.

[38]Aubry, N., Holmes, P., Lumley, J. L., and Stone, E., "The dynamics of coherent structures in the wall region of a turbulent boundary layer," *Journal of Fluid Mechanics*, Vol. 192, 1988, pp. 115–173.

[39]Zheng, X., *A low dimensional description of the axisymmetric jet mixing layer*, Ph.D. thesis, Clarkson University, 1990.

[40]Rempfer, D., "On Low-Dimensional Galerkin Models for Fluid Flow," *Theoret. Comput. Fluid Dynamics*, Vol. 14, 2000, pp. 75–88.

[41]Ukeiley, L. S., Cordier, L., Manceau, R., Delville, J., Glauser, M. N., and Bonnet, J.-P., "Examination of large-scale structures in a turbulent plane mixing layer. Part 2. Dynamical systems model," *Journal of Fluid Mechanics*, Vol. 441, 2001, pp. 67–108.

[42]Rajaee, M., Karlsson, S. K. F., and Sirovich, L., "Low-dimensional description of free-shear-flow coherent structures and their dynamical behaviour," *Journal of Fluid Mechanics*, Vol. 258, 1994, pp. 1–29.

[43]Rowley, C. R., *Modeling, Simulation, and Control of Cavity Flow Oscillations*, Ph.D. thesis, California Institute of Technology, 2002.

[44]Samimy, M., Debiasi, M., Caraballo, E., Serrani, A., Yuan, X., Little, J., and Myatt, J. H., "Feedback control of subsonic cavity flows using reduced-order models," *Journal of Fluid Mechanics*, Vol. 579, 2007, pp. 315–346.

[45]Caraballo, E., Little, J., Debiasi, M., and Samimy, M., "Development and Implementation of an Experimental-Based Reduced-Order Model for Feedback Control of Subsonic Cavity Flows," *ASME J. Fluids Enrng.*, Vol. 129, No. 7, 2007, pp. 813–824.

[46]Kim, J., Afshari, A., Bodony, D. J., and Freund, J. B., "LES Investigation of a Mach 1.3 Jet With and Without Plasma Actuators," *47th AIAA Aerospace Sciences Meeting, AIAA Paper 2009-290*, 2009.

[47]Kleinman, R. R., Bodony, D. J., and Freund, J. B., "Numerical Modeling of Plasma Actuators in High Speed Jets," *15th AIAA/CEAS Aeroacoustics Conference, AIAA Paper 2009-3190*, 2009.

[48]Gaitonde, D. V., "Simulation of Supersonic Nozzle Flows with Plasma-based Control," *39th Fluid Dynamics Conference and Exhibit, AIAA Paper 2009-4187*, 2009.

[49]Freund, J. B., "Noise sources in a low-Reynolds-number turbulent jet at Mach 0.9," *Journal of Fluid Mechanics*, Vol. 438, No. 1, 2001, pp. 277–305.

[50]Kastner, J., Samimy, M., Hileman, J., and Freund, J. B., "Comparison of Noise Mechanisms in High and Low Reynolds Number High-Speed Jets," *AIAA Journal*, Vol. 44, No. 10, 2006, pp. 2251–2258.

[51]Ma, X. and Karniadakis, G. M., "A low-dimensional model for simulating three-dimensional cylinder flow," *Journal of Fluid Mechanics*, Vol. 458, 2002, pp. 181–190.

[52]Sirovich, L., "Turbulence and the dynamics of coherent structures, Parts I-III," *Q. Appl. Math.*, Vol. XLV, No. 3, 1987, pp. 561–590.

[53]Tinney, C. E., Ukeiley, L. S., and Glauser, M. N., "Low-dimensional characteristics of a transonic jet. Part 2. Estimate and far-field prediction," *Journal of Fluid Mechanics*, Vol. 615, 2008, pp. 53–92.

[54]George, W. K., "Insight into the dynamics of coherent structures from a proper orthogonal decomposition," *Proc. Symp. on Near Wall Turbulence, Dubrovnik, Yugoslavia*, 1988.

[55]Bendat, J. S. and Piersol, A. G., *Engineering Applications of Correlation and Spectral Analysis*, John Wiley, 3rd ed., 2000.

[56]Moin, P. and Moser, R. D., "Characteristic-eddy decomposition of turbulence in a channel," *Journal of Fluid Mechanics*, Vol. 200, 1989, pp. 471–509.

[57]Glauser, M. N. and George, W. K., "Orthogonal decomposition of the axisymmetric jet mixing layer including azimuthal dependence," *Advances in turbulence*, edited by G. Comte-Bellot and J. Mathieu, Springer-Verlag, 1987, pp. 357–366.

[58]Adrian, R. J., "On the role of conditional averages in turbulence theory," *Turbulence in Liquids; Proc. 4th Biennal Symp. Missouri, USA (A77-40426 18-34), Princeton, NJ*, Science Press, 1977, pp. 323–332.

[59]Adrian, R. A., "Stochastic Estimation of Conditional Structure: a Review," *Applied Scientific Research*, Vol. 53, 1994, pp. 291–303.

[60]Ewing, D. and Citriniti, J. H., "Examination of a LSE/POD Complementary Technique using Single and Multi-Time Information in the Axisymmetric Shear Layer," *Proceedings of the IUTAM Symposium on simulation and identification of organized structures in flows, Lyngby, Denmark, 25-29 May 1997*, edited by J. Sorensen, E. Hopfinger, and N. Aubry, Kluwer Academic Press, 1999, pp. 375–384.

[61]Bonnet, J.-P., Cole, D. R., Delville, J., Glauser, M. N., and Ukeiley, L. S., "Stochastic estimation and proper orthogonal decomposition: Complementary techniques for identifying structure," *Experiments in Fluids*, Vol. 17, No. 5, 1994, pp. 307–314.

[62]Tinney, C. E. and Glauser, M. N., "The Modified Complementary Technique applied to the Mach 0.85 axisymmetric jet for noise prediction," *13th AIAA/CEAS Aeroacoustics Conference, AIAA Paper 2007-3663*, 2007.

[63]Tinney, C. E., Coiffet, F., Delville, J., Hall, A. M., Jordan, P., and Glauser, M. N., "On spectral linear stochastic estimation," *Experiments in Fluids*, Vol. 41, No. 5, 2006, pp. 763–775.

[64]Tinney, C. E., Jordan, P., Hall, A. M., Delville, J., and Glauser, M. N., "A time-resolved estimate of the turbulence and sound source mechanisms in a subsonic jet flow," *Journal of Turbulence*, Vol. 8, No. 7, 2007, pp. 1–20.

[65]De Boor, C., *A Practical Guide to Splines*, Springer-Verlag, New York, 1978.

[66]Schlichting, H., *Boundary-Layer Theory*, McGraw Hill, 1968.

[67]Deane, A. E., Kevrekidis, I. G., and Karniadakis, G. E. Orszag, S. C., "Low-dimensional models for complex geometry flows: Application to grooved channels and circular cylinders," *Physics of Fluids A*, Vol. 3, No. 10, 1991, pp. 2337–2354.

[68]Rempfer, D. and Fasel, H. F., "Dynamics of three-dimensional coherent structures in a flat-plate boundary layer," *Journal of Fluid Mechanics*, Vol. 275, 1994, pp. 257–283.

[69]Rowley, C. R., "Model reduction for compressible flows using POD and Galerkin projection," *Physica D*, Vol. 189, 2004, pp. 115–129.

[70]Noack, B. R., Papas, P., and Monkewitz, P., "The need for a pressure-term representation in empirical Galerkin models of incompressible shear flows," *Journal of Fluid Mechanics*, Vol. 523, 2005, pp. 339–365.

[71]Cazemier, W., Verstappen, R. W. C. P., and Veldman, A. E. P., "Proper orthogonal decomposition and low-dimensional models for driven cavity flows," *Physics of Fluids*, Vol. 10, No. 7, 1998, pp. 1685–1699.

[72]Couplet, M., Sagaut, P., and Basdevant, C., "Intermodal energy transfers in a proper orthogonal decomposition-Galerkin representation of a turbulent separated flow," *Journal of Fluid Mechanics*, Vol. 491, 2003, pp. 275–284.

[73]Arndt, R. E. A., Long, D. F., and Glauser, M. N., "The proper orthogonal decomposition of pressure fluctuations surrounding a turbulent jet," *Journal of Fluid Mechanics*, Vol. 340, No. 1, 1997, pp. 1–33.

[74]Coiffet, F., Jordan, P., Delville, J., Gervais, Y., and Ricaud, F., "Coherent structures in subsonic jets: a quasi-irrotational source mechanism?" *International Journal of Aeroacoustics*, Vol. 5, No. 1, 2006, pp. 67–89.

[75]Caraballo, E., Samimy, M., and DeBonis, J., "Low Dimensional Modeling of Flow for Closed-Loop Flow Control," *41st AIAA Aerospace Sciences Meeting and Exhibit, AIAA Paper 2003-0059*, 2003.